Monthly Notices
of the
ROYAL ASTRONOMICAL SOCIETY

MNRAS **481,** 2273–2298 (2018)
Advance Access publication 2018 August 29

doi:10.1093/mnras/sty2312

The evolution of X-ray bursts in the 'Bursting Pulsar' GRO J1744–28

J. M. C. Court [1]★ D. Altamirano,[1] A. C. Albayati,[2] A. Sanna [3] T. Belloni,[4] T. Overton,[5] N. Degenaar,[6] R. Wijnands,[6] K. Yamaoka,[7] A. B. Hill [8,1] and C. Knigge[1]

[1]*School of Physics and Astronomy, University of Southampton, Southampton SO17 1BJ, UK*
[2]*School of Physics and Astronomy, Queen Mary University of London, London E1 4NS, UK*
[3]*Dipartimento di Fisica, Università degli Studi di Cagliari, SP Monserrato-Sestu km 0.7, I-09042 Monserrato, Italy*
[4]*Osservatorio Astronomico di Brera, Via E. Bianchi 46, I-23807 Merate (LC), Italy*
[5]*Department of Physics, Royal Holloway, University of London, Egham TW20 0EX, UK*
[6]*Anton Pannekoek Institute for Astronomy, University of Amsterdam, Science Park 904, NL-1098 XH, Amsterdam, the Netherlands*
[7]*Department of Physics, Nagoya University, Aichi 464-8602, Japan*
[8]*HAL24K, Building B.3, Johan Huizingalaan 400, NL-1066 JS Amsterdam, the Netherlands*

Accepted 2018 August 20. Received 2018 August 17; in original form 2018 April 30

ABSTRACT

GRO J1744–28, commonly known as the 'Bursting Pulsar', is a low-mass X-ray binary containing a neutron star and an evolved giant star. This system, together with the Rapid Burster (MXB 1730-33), are the only two systems that display the so-called type II X-ray bursts. These types of bursts, which last for tens of seconds, are thought to be caused by viscous instabilities in the disc; however, the type II bursts seen in GRO J1744–28 are qualitatively very different from those seen in the archetypal type II bursting source, the Rapid Burster. To understand these differences and to create a framework for future study, we perform a study of all X-ray observations of all three known outbursts of the Bursting Pulsar which contained type II bursts, including a population study of all type II X-ray bursts seen by *RXTE*. We find that the bursts from this source are best described in four distinct phenomena or 'classes' and that the characteristics of the bursts evolve in a predictable way. We compare our results with what is known for the Rapid Burster and put out results in the context of models that try to explain this phenomena.

Key words: accretion, accretion discs – instabilities – stars: neutron – X-rays: binaries – X-rays: individual: GRO J1744-28 – X-rays: individual: MXB 1730-335.

1 INTRODUCTION

Low-mass X-ray binaries (hereafter LMXBs) are extremely dynamic astrophysical systems, which exhibit high-amplitude X-ray variability on time-scales of milliseconds to years. In these systems a compact object accretes matter from a stellar companion, either via a stellar wind or via Roche lobe overflow. The donated matter spirals in towards the compact object, forming an accretion disc of matter which heats up by friction to temperatures of $\gtrsim$1 keV.

LMXBs are excellent laboratories in which to explore the physics of how matter behaves in extreme physical conditions. In addition to extreme temperatures, the inner portion of an accretion disc is a region of extreme gravity, gas pressure, and photon pressure. If the primary object in the binary is a neutron star, these systems also contain regions of extreme magnetic fields.

Many LMXBs containing a neutron star are known to exhibit 'bursts'; discrete periods of increased X-ray emission over time-scales of seconds. These bursts are generally categorized as either type I or type II, depending on the profile of the burst and its spectral evolution (Hoffman, Marshall & Lewin 1978; Lewin, van Paradijs & Taam 1993). Type I bursts are caused by accreted matter on the surface of the neutron star reaching a critical pressure and temperature which triggers runaway thermonuclear burning (see e.g. Lewin et al. 1993; Strohmayer & Bildsten 2006). They appear in X-ray light curves as a sudden increase in intensity, followed by a power-law decay (in't Zand et al. 2014), over a time-scale of a few tens of seconds.

Type II bursts are believed to be caused by viscous instabilities in the accretion disc (Lewin et al. 1976a). However, the exact details of the mechanism responsible for type II bursts remain unclear. This type of bursts is more varied in its phenomenological appearance, ranging from near-Gaussian in shape over time-scales of $<$1 s to broad flat-topped light-curve features which last for $\sim$100 s (e.g. Bagnoli et al. 2015).

Type I X-ray bursts are seen in data from over a hundred neutron star LMXBs, while regular type II bursts have only been unambiguously identified in two sources: the 'Rapid Burster'

★ E-mail: J.M.Court@soton.ac.uk

© 2018 The Author(s)
Published by Oxford University Press on behalf of the Royal Astronomical Society

Downloaded from https://academic.oup.com/mnras/article-abstract/481/2/2273/5086081 by INAF Brera Milano (Osservatorio Astronomico di Brera) user on 20 February 2019

MXB 1730-335 (Lewin et al. 1976a) and the 'Bursting Pulsar' GRO J1744–28 (Kouveliotou et al. 1996). Isolated type II bursts may have also been observed in at least one additional X-ray Binary (SMC X-1, Angelini, White & Stella 1991), but the identification of these features remains unclear.

The type II bursting behaviour in the Rapid Burster has been extensively studied (see e.g. Lewin et al. 1976a; Hoffman et al. 1978). Bagnoli et al. (2015) performed a full population study of all type II bursts observed in this object by the *Rossi X-ray Timing Explorer* (*RXTE*; Bradt, Rothschild & Swank 1993). Their results suggest that gating of the accretion by a strong magnetic field plays some role in the creation of type II bursts. To further probe the physics behind type II X-ray bursts, in this paper we perform a similar population study on bursts from the Bursting Pulsar.

The Bursting Pulsar (Paciesas et al. 1996) is a system containing a neutron star and a G or K class evolved companion star (e.g. Sturner & Dermer 1996; Gosling et al. 2007; Masetti et al. 2014). The system lies at a distance of ∼4–8 kpc in the direction of the Galactic centre (e.g. Kouveliotou et al. 1996; Gosling et al. 2007; Sanna et al. 2017a), and it is the only known pulsar that regularly displays type II bursts. The Bursting Pulsar accretes at a high rate: by estimating the accretion rate of the object by measuring how fast the pulsar spins up, Sturner & Dermer 1996 found that the Bursting Pulsar accretes at close to the Eddington limit for a neutron star.

Unlike in the Rapid Burster, unambiguous type I bursts have never been observed from the Bursting Pulsar (e.g. Giles et al. 1996, however see also Lamb, Miller & Taam 1996; Doroshenko et al. 2015). Type II bursts were first identified upon discovery in 1995 by the Burst and Transient Source Experiment (BATSE) aboard the *Compton Gamma Ray Observatory* (*CGRO*; Gehrels, Chipman & Kniffen 1994). Additional outbursts have occurred irregularly; specifically in 1997 and 2014 (Woods et al. 1999; Kennea, Kouveliotou & Younes 2014). An additional outburst may have occurred in 2017 (Sanna et al. 2017b), but it was significantly less luminous than previous outbursts and the Bursting Pulsar did not transition to the soft state (such events are referred to as 'failed outbursts' or 'failed state-transition outbursts', see e.g. Sturner & Shrader 2005).

Previous work by Giles et al. (1996) indicated that type II bursts in the 1995–1996 outburst of the Bursting Pulsar could be separated into a number of distinct populations based on peak flux. This is a notable difference from the Rapid Burster, in which all type II bursts have peak fluxes approximately equal to or less than object's Eddington Luminosity (Tan et al. 1991). In this paper, we expand on the work of Giles et al. (1996) and analyse *RXTE*, *NuSTAR*, *Chandra*, *XMM–Newton*, *Swift*, and *INTEGRAL* data to fully quantify the population of type II bursts in the Bursting Pulsar during all outbursts in which they were observed. We study how the bursting in this object evolves over time throughout each outburst, and we link this behaviour to the long-term evolution of the source. We also perform basic timing, morphology, and spectral analysis on bursts, to try and understand the physical processes behind these phenomena.

2 DATA AND DATA ANALYSIS

Since discovery, the Bursting Pulsar has undergone three bright outbursts, which began in 1995, 1997, and 2014. We refer to these outbursts as Outbursts 1, 2, and 3. We do not consider the outburst in 2017 in this paper, as no type II bursts were observed during this time, nor do we analyse data taken while the source was in quiescence. See Daigne et al. (2002), Wijnands & Wang (2002), and Degenaar et al. (2012) for studies of the Bursting Pulsar during quiescence.

We analysed data from all X-ray instruments which observed the Bursting Pulsar during these outbursts. Specifically, we analysed light curves, the evolution of hardness ratios as a function of time and of count rate, and performed statistical analysis of properties associated with each individual burst.

2.1 *RXTE*

We analysed data from the Proportional Counter Array (PCA; Jahoda et al. 1996) aboard *RXTE* corresponding to the Outbursts 1 and 2 of the Bursting Pulsar. This in turn corresponded to observation IDs starting with 10401-01, 20077-01, 20078-01, 20401-01, and 30075-01, between MJDs 50117 and 51225. This resulted in a total of 743 ks of data over 300 observations, which we have listed in Appendix A. Light-curve data were extracted from `fits` files using `FTOOLS`.[1] Errors were calculated and quoted at the 1 σ level.

We also use data from the All-Sky Monitor (ASM; Levine et al. 1996) to monitor the long-term evolution of the source. ASM data were taken from MIT's ASM Light Curves Overview website.[2]

2.1.1 *Long-term evolution*

To analyse the long-term evolution of the source during its outbursts, we extracted 2–16 keV count rates from the *Standard2* data in each observation. Following Altamirano et al. (2008b), we normalized the intensity estimated in each observation by the intensity of the Crab nebula, using the Crab observation that is the closest in time but within the same PCA gain epoch as the observation in question (see Jahoda et al. 2006).

2.1.2 *Burst identification and analysis*

To perform population studies on the type II bursts in the Bursting Pulsar, we first extracted light curves from the `Standard1` data in each observation, as these data are available for all *RXTE* observations. We used our own software[3] to search these light curves and return a list of individual bursts, using the algorithm described in appendix A of Court et al. (2017). We manually cleaned spurious detections from our sample. We defined a 'burst' as an event that lasted at least 3 s during which the 1 s binned count rate exceeded three standard deviations above the persistent emission level and reached a maximum of at least five standard deviations above the persistent emission level. We did not subtract background, as all count rate-related parameters we analyse are persistent emission subtracted, automatically removing background contribution.

During the analysis, we discovered a number of different 'classes', similar to the multiple classes of burst described by Giles et al. (1996). Our classes varied significantly in terms of overall structure, and as such needed to be treated separately; we show representative light curves from our classes in Fig. 2. These classes were separated from one another by a number of criteria including

[1] https://heasarc.gsfc.nasa.gov/ftools/ftools_menu.html
[2] http://xte.mit.edu/ASM_lc.html
[3] https://github.com/jmcourt/pantheon (Court 2017),

Downloaded from https://academic.oup.com/mnras/article-abstract/481/2/2273/5086081 by INAF Brera Milano (Osservatorio Astronomico di Brera) user on 20 February 2019

peak count rate and recurrence time (the time between peaks of consecutive bursts).

The vast majority of detected bursts resembled the type II seen in the Rapid Burster (referred to as 'Normal Bursts' in Section 3) in terms of shape, duration, and amplitude. We rebinned the data corresponding to these Normal Bursts to 0.5 s. We sampled the persistent emission before the burst, and defined the start of the burst as the first point at which count rate exceeded five standard deviations above the persistent emission before the burst. The end of the burst was defined similarly, but instead sampling the persistent emission after the burst; by doing this, we avoid making the implicit assumption that the persistent emission is equal before and after the burst. We fitted phenomenologically motivated light-curve models to each of these bursts (described in detail in Section 3.3.2), and used these fits to extract a number of parameters which characterize the shape and energetics of a burst (such as burst duration, total photon counts associated with a burst, and persistent emission count rate).

Due to the high peak count rates of Normal Bursts, data were affected by dead time (compare e.g. *GRANAT* data presented in Sazonov, Sunyaev & Lund 1997). We calculate the approximate dead-time factors (DTFs) for a number of the brightest Normal Bursts in our sample, using 1 s binned data, using the following formula in the *RXTE* Cookbook[4]:

$$\Delta = \frac{C_{\rm Xe} + C_{\rm Vp} + C_{\rm Rc} + 15C_{\rm VL}}{N_{\rm PCU}} \times 10^{-5}, \quad (1)$$

where Δ is the fractional detector dead time, $C_{\rm Xe}$ is the Good Xenon count rate, $C_{\rm Vp}$ is the coincident event count rate, $C_{\rm Rc}$ is the propane layer count rate, $C_{\rm VL}$ is the very large event count rate, and $N_{\rm PCU}$ is the number of PCUs active at the time.

We estimate that dead-time effects reduce the peak count rates by no more than ∼12 per cent; however, due to the sharply peaked nature of bursts from the Bursting Pulsar, the dead-time effect depends on the binning used. Due to this ambiguity we do not correct for dead time in Normal Bursts. The dead-time corrections required for the count rates seen in other classes of burst are minimal, as they are orders of magnitude fainter (Giles et al. 1996).

To test for correlations between parameters in a model-independent way, we used the Spearman's Rank correlation coefficient (as available in `scipy`, Jones et al. 2001). This metric only tests the hypothesis that an increase in the value of one parameter is likely to correspond to an increase in the value of another parameter, and it is not affected by the shape of the monotonic correlation to be measured. Although dead-time effects lead to artificially low count rates being reported, a higher intensity still corresponds to a higher reported count rate. As such, using this correlation coefficient removed the effects of dead time on our detection of any correlations.

To calculate the distribution of recurrence times between consecutive bursts, we considered observations containing multiple bursts. If fewer than 25 s of data gap exists between a pair of bursts, we considered them to be consecutive and added their recurrence time to the distribution. We choose this maximum gap size as this is approximately the time-scale over which a Normal Burst occurs.

To perform basic phenomenological analysis of the spectral behaviour of these bursts, we divided our data into two energy bands when `SB_62us_0_23_500ms` and `SB_62us_24_249_500ms` mode data were available: A (PCA channels 0–23, corresponding to ∼2–7 keV[5]) and B (channels 24–249, corresponding to ∼8–60 keV[6]). The evolution of colour (defined as the ratio of the count rates in B and A) throughout a burst could then be studied. Due to the very high count rates during Normal Bursts, we did not correct for background. During fainter types of burst we estimate the background in different energy bands by subtracting count rates from *RXTE* observation 30075-01-26-00 of this region, when the source was inactive. Unlike using the *RXTE* background model, this method subtracts the contributions from other sources in the field. However, as it is unclear whether any of the rest of these sources are variable, the absolute values of colours we quote should be treated with caution. We created hardness-intensity diagrams to search for evidence of hysteretic loops in hardness-intensity space.

Following Bagnoli et al. (2015), we used the total number of persistent emission-subtracted counts as a proxy for fluence for all bursts other than Normal Bursts. As the contribution of the background does not change much during a single observation, this method also automatically subtracts background counts from our results.

2.1.3 *Detecting pulsations*

The Bursting Pulsar is situated in a very dense region of the sky close to the Galactic centre, and so several additional objects also fall within the 1° *RXTE*/PCA field of view. Therefore, it is important to confirm that the variability we observe in our data does in fact originate from the Bursting Pulsar.

To ascertain that all bursts considered in this study are from the Bursting Pulsar, we analyse the coherent X-ray pulse at the pulsar spin frequency to confirm that the source was active. We first corrected the photon time of arrivals (ToA) of the *RXTE*/PCA data set, and barycentre this data using the `faxbary` tool (DE-405 Solar System ephemeris). We corrected for the binary motion by using the orbital parameters reported by Finger et al. (1996).

For each PCA observation, we investigated the presence of the ∼2.14 Hz coherent pulsation by performing an epoch-folding search of the data using 16 phase bins and starting with the spin frequency value $\nu = 2.141004$ Hz, corresponding to the spin frequency measured from the 1996 outburst of the source (Finger et al. 1996), with a frequency step of 10^{-5} Hz for 10001 total steps. We detected X-ray coherent pulsations in all PCA observations performed during Outbursts 1 and 2.

2.2 *Swift*

In this study, we made use of data from the X-Ray Telescope (XRT; Burrows et al. 2003) and the Burst Alert Telescope (BAT; Krimm et al. 2013) aboard the Neil Gehrels Swift Observatory (*Swift*; Gehrels 2004). We extracted a long-term 0.3–10 keV *Swift*/XRT light curve of Outburst 3 using the light-curve generator provided by the UK Swift Science Data Centre (UKSSDC; Evans et al. 2007). We also make use of *Swift*/BAT light curves from the Swift/BAT Hard X-ray Transient website[7] (see Krimm et al. 2013).

[4] https://heasarc.gsfc.nasa.gov/docs/xte/recipes/pca_deadtime.html

[5] In *RXTE* gain epoch 1, corresponding to dates before MJD 50163. This corresponds to ∼2–9 keV in epoch 2 (MJDs 50163–50188) and ∼2–10 keV in epoch 3 (MJDs 50188–51259).

[6] In *RXTE* gain epoch 1. This corresponds to ∼9–60 keV in epoch 2 and ∼10–60 keV in epoch 3.

[7] https://swift.gsfc.nasa.gov/results/transients/

Downloaded from https://academic.oup.com/mnras/article-abstract/481/2/2273/5086081 by INAF Brera Milano (Osservatorio Astronomico di Brera) user on 20 February 2019

Table 1. Information on the three *Chandra* observations of the Bursting Pulsar during Outburst 3. All other observations of the Bursting Pulsar in the *Chandra* archive were obtained at times that the source was in quiescence.

OBSID	Exposure (ks)	MJD	Reference
16596	10	56719	Younes et al. (2015)
16605	35	56745	Degenaar et al. (2014)
16606	35	56747	Degenaar et al. (2014)

2.3 *INTEGRAL*

We also made use of data from the Imager on Board *INTEGRAL* (Winkler et al. 2003). We extracted 17.3–80 keV IBIS/ISGRI light curves of the Bursting Pulsar during Outburst 3 using the *INTEGRAL* Heavens portal. This is provided by the *INTEGRAL* Science Data Centre (Lubiński 2009).

2.4 *Chandra*

The Bursting Pulsar was targeted with *Chandra* (Weisskopf 1999) three times during Outburst 3 (Table 1). One of these observations (OBSID 16596) was taken simultaneously with a *NuSTAR* observation (80002017004). In all three observations, data were obtained with the High Energy Transmission Grating (HETG), where the incoming light was dispersed onto the ACIS-S (Garmire et al. 2003) array. The ACIS-S was operated in continued clocking (CC) mode to minimize the effects of pile-up. The *Chandra*/HETG observations were analysed using standard tools available within `ciao` v. 4.5 (Fruscione et al. 2006). We extracted 1 s binned light curves from the `evt2` data using `dmextract`, where we combined the first-order positive and negative grating data from both the Medium Energy Grating (MEG; 0.4–5 keV) and the High Energy Grating (HEG; 0.8–8 keV).

2.5 *XMM–Newton*

A single pointed *XMM–Newton* observation of the Bursting Pulsar was taken during Outburst 3 on MJD 56722 (OBSID 0729560401) for 85 ks. We extracted a 0.5–10 keV light curve from EPIC-PN at 1 s resolution using `xmmsas` version 15.0.0. During this observation, EPIC-PN was operating in Fast Timing mode. We use EPIC-PN, as the statistics are better than in MOS1 or MOS2.

2.6 *Suzaku*

Suzaku (Mitsuda et al. 2007) observed the Bursting Pulsar once during Outburst 3 on MJD 56740 (OBSID 908004010).

To create a light curve, we reprocessed and screened data from the X-ray Imaging Spectrometer (XIS; Koyama et al. 2007) using the `aepipeline` script and the latest calibration database released on 2016 June 7. The attitude correction for the thermal wobbling was made by `aeattcor2` and `xiscoord` (Uchiyama et al. 2008). The source was extracted within a radius of 250 pixels corresponding to 260 arcmin from the image centre. The background was extracted from two regions near either end of the XIS chip, and subtracted from the source.

2.7 *NuSTAR*

NuSTAR (Harrison et al. 2013) consists of two grazing-incident X-ray telescopes. These instruments only observed the Bursting Pulsar three times during its outbursts, all times in Outburst 3. One of these observations was taken while the Bursting Pulsar was not showing X-ray bursts, and the other two are shown in Table 2. We extracted light curves from both of these observations using `nupipeline` and `nuproducts`, following standard procedures.[8]

Table 2. Information on the two *NuSTAR* observations of the Bursting Pulsar during the main part of Outburst 3.

OBSID	Exposure (ks)	MJD	Reference
80002017002	29	56703	D'Aì et al. (2016)
80002017004	9	56719	Younes et al. (2015)

3 RESULTS

3.1 Outburst evolution

We show the long-term monitoring light curves of Outbursts 1,2 and 3 in Fig. 1, as well as mark the dates of pointed observations with various instruments.

The Bursting Pulsar was discovered already in outburst on 1995 December 12 (Fishman et al. 1995); BATSE data suggest that this outburst began several days earlier on December 3 (Paciesas et al. 1996; Bildsten et al. 1997). The main outburst ended around 1996 May 10 (Woods et al. 2000). We show the global light curve of this outburst in Fig. 1, Panel 1. As *RXTE* did not observe the object before or during the peak of Outburst, we can only obtain a lower limit of ∼1.75 Crab for the peak 2–16 keV flux.

There are at least two major rebrightening events in the tail of Outburst 1, which can be seen clearly in Fig. 1 centred at MJDs of ∼50235 and ∼50280. During these rebrightening events, the 2–16 keV flux peaked at ∼0.10 and ∼0.18 Crab, respectively.

Outburst 2 began on 1996 December 1 and ended around 1997 April 7 (Woods et al. 1999). The 2–16 keV flux peaked at 1.02 Crab on MJD 50473; we show the global light curve of this outburst in Fig. 1, Panel 2. Type II bursts are seen in *RXTE*/PCA light curves from Outburst 2 between MJDs 50466 and 50544. One rebrightening event occurred during the tail of Outburst 2, centred at an MJD of ∼50615 with a peak 2–16 keV flux of ∼54 mCrab. A second possible rebrightening event occurs at MJD 50975, with a peak 2–16 keV flux of 11 mCrab, but the cadence of *RXTE*/PCA observations was too low to unambiguously confirm the existence of a reflare at this time.

Outburst 3 began on 2014 January 31 (Kennea et al. 2014; Negoro et al. 2014) and ended around April 23 (e.g. D'Aì et al. 2015). The daily 0.3–10 keV *Swift*/XRT rate peaked at 81 cts s^{-1} on MJD 56729, corresponding to 0.4 Crab. We show the global light curve of this outburst in Fig. 1, Panel 3.

During the main part of Outburst 3, *Swift*, *XMM–Newton*, and *Suzaku* made one pointed observation each, *Chandra* made four observations, and *NuSTAR* made three observations. The *Chandra* observation on 2014 March 3 was made simultaneously with one of the *NuSTAR* observations (see Younes et al. 2015). After the main part of the outburst, the source was not well monitored, although it remained detectable by *Swift*/BAT, and it is unclear whether any rebrightening events occurred. A single *NuSTAR* observation was made during the outburst tail on 2014 August 14.

As can be seen in Fig. 1, the main section of all three outburst follow a common profile, over a time-scale of ∼150 d. A notable

[8] See https://www.cosmos.esa.int/web/xmm-newton/sas-threads.

Downloaded from https://academic.oup.com/mnras/article-abstract/481/2/2273/5086081 by INAF Brera Milano (Osservatorio Astronomico di Brera) user on 20 February 2019

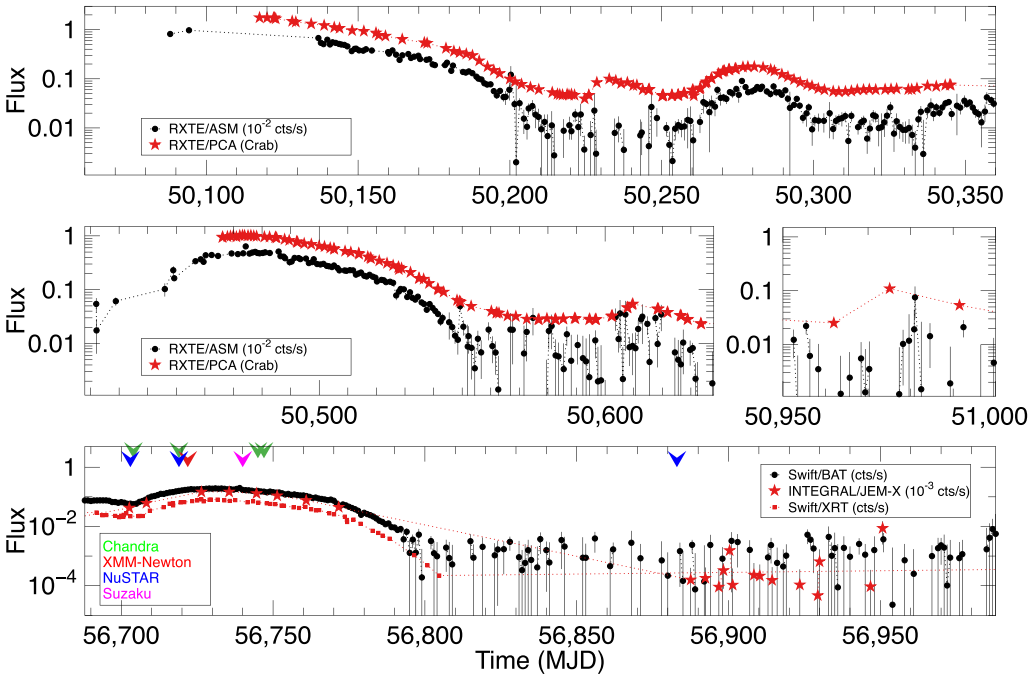

Figure 1. Comparisons of the three outbursts of the Bursting Pulsar reported in this paper. Times corresponding to pointed observations with *Chandra*, *NuSTAR*, *Suzaku*, *Swift*, and *XMM–Newton* are marked.

difference between outbursts 1 and 2 is the number of rebrightening events; while we find two rebrightening events associated with Outburst 1, we only find one associated with Outburst 2 unless we assume the event at MJD 50975 is associated with the outburst. Additionally, Outburst 2 was at least a factor ∼1.7 fainter at its peak than Outburst 1 (see also Woods et al. 1999), while Outburst 3 was a factor of $\gtrsim$4 fainter at peak than Outburst 1.

3.1.1 Pulsations

We found pulsations in PCA data throughout the entirety of Outbursts 1 and 2. This confirms that the Bursting Pulsar was active as an X-ray pulsar in all of our observations, leading us to conclude that all the types of type II bursts we see are from the Bursting Pulsar.

3.1.2 Bursting behaviour

Bursts are seen in *RXTE*/PCA light curves from the start of the Outburst 1 (e.g. Kouveliotou et al. 1996). These type II bursts occur until around MJD 50200, as the source flux falls below ∼0.1 Crab in the 2–16 keV band.

During the latter part of the first rebrightening after Outburst 1, between MJDs 50238 and 50246, we found type II like bursts with amplitudes ∼2 orders of magnitude smaller than those found during the main outburst event. These gradually increased in frequency throughout this period of time until evolving into a period of highly structured variability which persisted until MJD 50261.

In Outburst 2, we found type II bursts occurring between MJDs ∼50466 and 50542. Low-amplitude type II like bursts are seen during the latter stages of the main outburst, between MJDs 50562 and 50577. These again evolve into a period of highly structured variability; this persists until MJD 50618, just after the peak of the rebrightening event.

High-amplitude type II bursts were also seen in Outburst 3 (e.g. Linares et al. 2014). As no soft ($\lesssim$10 keV) X-ray instrument was monitoring the Bursting Pulsar during the latter part of Outburst 3, it is unknown whether this Outburst showed the lower amplitude bursting behaviour seen at the end of Outbursts 1 and 2. Low amplitude bursting behaviour is not seen in the pointed *NuStar* observation which was made during this time.

3.2 Categorizing bursts

We find that bursts in the Bursting Pulsar fall into a number of discrete classes, light curves from which we show in Fig. 2. These classes are as follows:

(i) Normal Bursts (Fig. 2, Panel a): the brightest bursts seen from this source, with peak count 1 s binned rates of ∼10 000 cts s^{-1} PCU^{-1}, and recurrence time-scales of the order of ∼1000 s. These bursts are roughly Gaussian in shape with durations of ∼10 s, and are followed by a 'dip' in the persistent emission count rate with a duration of the order of 100 s (see also e.g. Giles et al. 1996).

(ii) Miniburst (Fig. 2, Panel b): faint bursts with 1 s binned peak count rates of ∼2 times the persistent emission count rate. Miniburst are variable, with duration time-scales between ∼5 and 50 s. These bursts are also sometimes followed by dips similar to those seen after Normal Bursts.

(iii) Mesobursts (Fig. 2, Panel c): type II like bursts. These bursts differ from Normal Bursts in that they do not show well-defined subsequent 'dips'. They are also fainter than Normal Bursts, with peak count 1 s binned count rates of ∼1000 cts s^{-1} PCU^{-1}. Their burst profiles show fast rises on time-scales of seconds, with slower decays and overall durations of ∼50 s. The structure of the bursts is very non-Gaussian, appearing as a small forest of peaks in light curves.

Downloaded from https://academic.oup.com/mnras/article-abstract/481/2/2273/5086081 by INAF Brera Milano (Osservatorio Astronomico di Brera) user on 20 February 2019

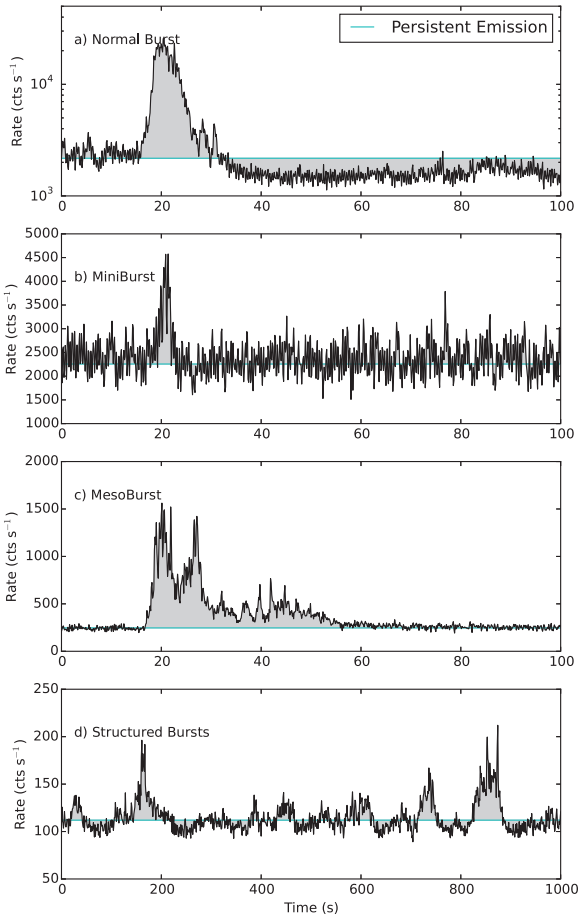

Figure 2. 2–49 keV light curves for the four classes of bursting behaviour identified in this paper: (a) Normal Burst, (b) Miniburst, (c) Mesoburst, (d) Structured Bursts. Note that Panel d is plotted with a different time scaling to the other panels so as to better show the behaviour of Structured Bursting. On all figures the median count rate, which we use as a proxy for the persistent emission, is plotted in cyan. Light curves a–c are binned to 0.125 s, while light curve d is binned to 1 s.

(iv) Structured Bursts (Fig. 2, Panel d): the most complex class of bursting behaviour we observe from the Bursting Pulsar, consisting of patterns of flares and dips in the X-ray light curve. The amplitudes of individual flares are similar to those of the faintest Mesobursts. The recurrence time-scale is of the order of the time-scale of an individual flare, meaning that is it difficult to fully separate individual flares of this class.

In the upper panel of Fig. 3, we show a histogram of persistent-emission-subtracted peak count rates for all Normal and Mesobursts observed by *RXTE*. We split these two classes based on the bimodal distribution in peak count rate as well as the lack of dips in Mesobursts.

In the lower panel of Fig. 3, we show the histogram of peak count rates for all Normal and Minibursts observed by *RXTE* as a fraction of the persistent emission at that time. We split these two classes based on the strongly bimodal distribution in fractional amplitude.

We also find six bursts with fast (∼1 s) rises and exponential decays that occur during the lowest flux regions of the outburst (≲50 mCrab). Strohmayer et al. (1997) and Galloway et al. (2008) have previously identified these bursts as being type I X-ray bursts from another source in the *RXTE* field of view. To show that these

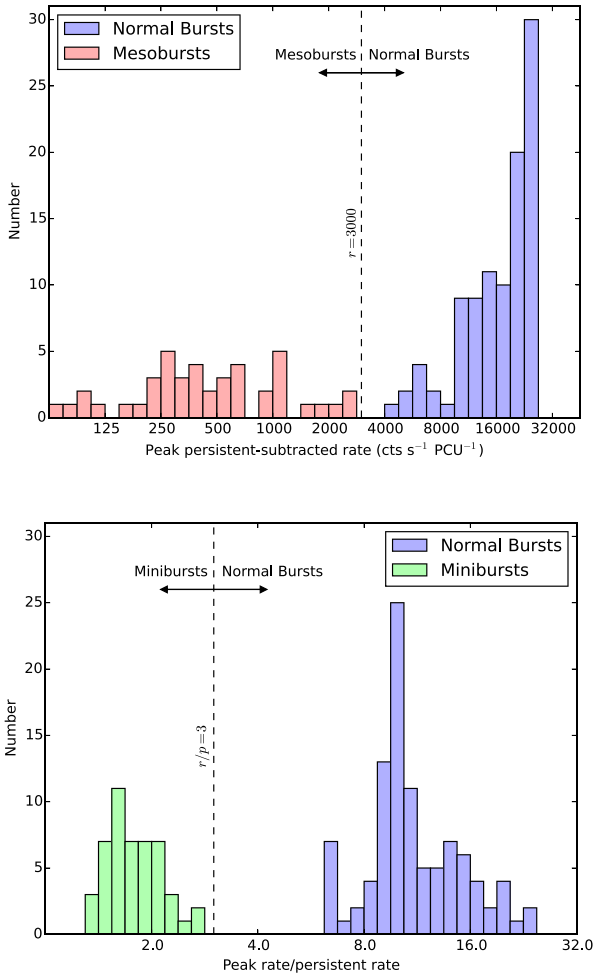

Figure 3. Upper panel: a histogram of the peak 1 s binned peak count rates of the joint population of all Normal and Mesobursts seen by *RXTE*. The dashed line indicates the position of the threshold above which we consider a type II like burst to be a Normal Burst. The resultant split of the population into Normal and Mesobursts is indicated by blue and red shading, respectively. The skewed shape of the distribution of Normal Bursts is due to the effects of dead time putting an effective cap on their maximum observed intensity. Lower panel: a histogram of the peak 1 s binned peak count rates of the joint population of all Normal and Minibursts seen by *RXTE*, divided by the persistent emission count rate at that time. The dashed line indicates the position of the threshold below which we consider a burst to be a Miniburst. The resultant split of the population into Normal and Minibursts is indicated by blue and green shading, respectively. Note that the x-axis of both plots is logarithmic, and so number density is not preserved.

unrelated type I bursts would not be confused with Minibursts, we add examples of the type I bursts to light curves from observations containing Minibursts. We find that the peak count rates in type I bursts are roughly equal to the amplitude of the noise in the persistent flux in these observations, hence they would not be detected by our algorithms.

We show when in Outbursts 1 and 2 each type of burst was observed in Figs 4 and 5, respectively. Normal Bursts and Minibursts (red) occur during the same periods of time from around the peak of an outburst until the persistent emission falls beneath ∼0.1 Crab; assuming an Eddington Limit of ∼1 Crab (e.g. Sazonov et al. 1997), this corresponds to an Eddington ratio of ∼0.1. After this point, bursting is not observed for a few tens of days. Mesobursts (blue)

Downloaded from https://academic.oup.com/mnras/article-abstract/481/2/2273/5086081 by INAF Brera Milano (Osservatorio Astronomico di Brera) user on 20 February 2019

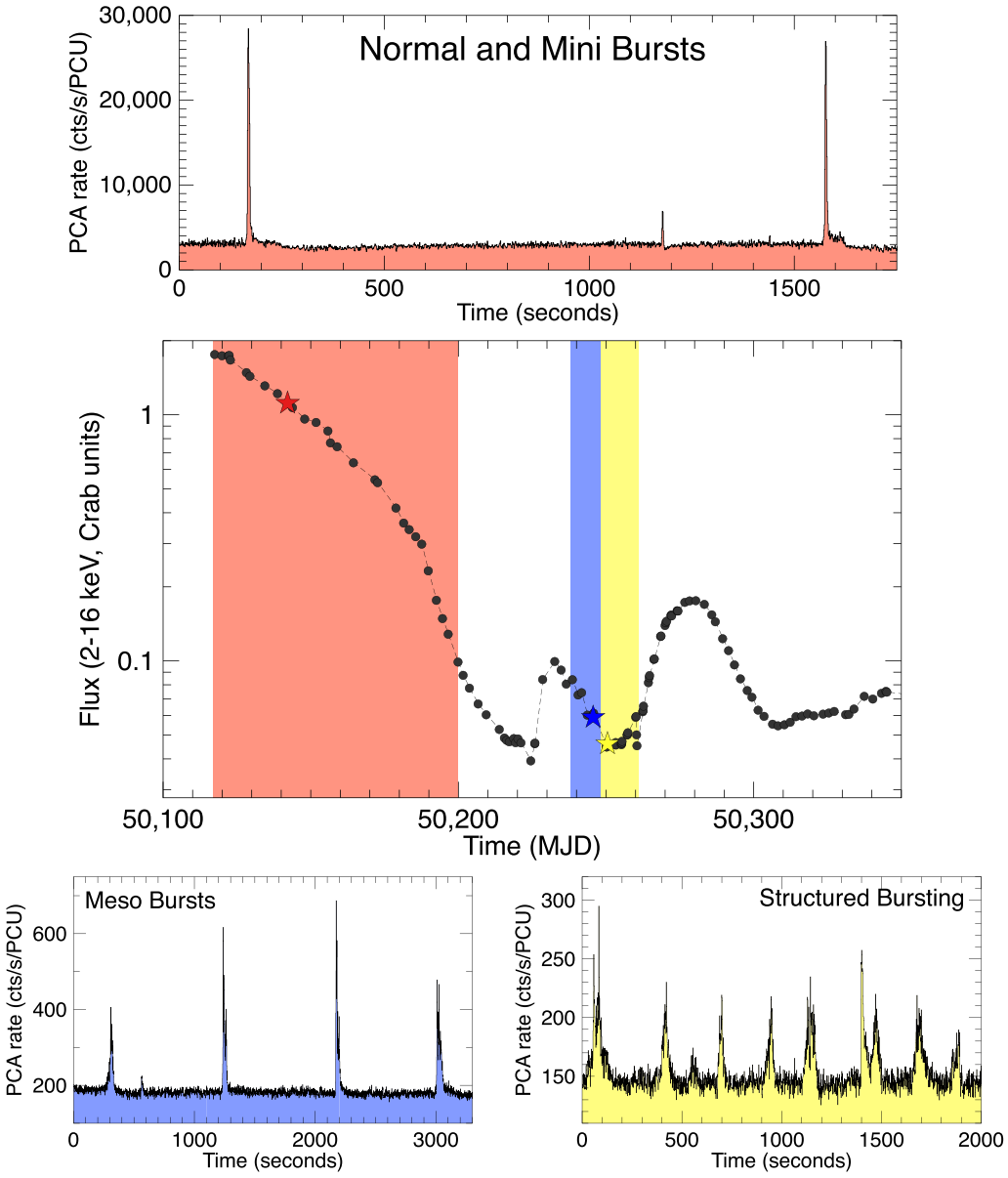

Figure 4. Central panel shows the global 2–16 keV *RXTE*/PCA light curve of the 1995–1996 outburst of the Bursting Pulsar, highlighting periods of time during which Mesobursts (blue), Structured Bursts (yellow), or Normal and Minibursts (red) are observed. A single Mesoburst was also observed on MJD 50253, during the period of the outburst highlighted in yellow (see Fig. 17). Other panels show example light curves which contain the aforementioned types of bursting behaviour. See Section 3.2 for a detailed treatment of burst classification. Fluxes reported in units of Crab.

begin at the end of a rebrightening event in Outburst 1 and during the final days of the main part of the outburst in Outburst 2. Structured Bursts (yellow) occur during the first part of a rebrightening event in both outbursts. Although there was a second rebrightening event after Outburst 1, neither Mesobursts nor Structured Bursts were observed at this time. Based on this separation, as well as differences in structure, we treat each class of burst separately below.

3.3 Normal Bursts

We define Normal Bursts as the set of all bursts with a persistent-emission-subtracted peak 1 s binned *RXTE*/PCA-equivalent count rate above 3000 cts s^{-1} PCU^{-1}. Normal Bursts account for 99 out of the 190[9] bursts identified for this study. They are observed during all three outbursts covered in this study. They occurred between MJDs 50117 and 50200 in Outburst 1, and between 50466 and 50542 in Outburst 2; during these intervals, *RXTE* observed the source for a total of 192 ks. See Table 3 to compare these with numbers for the other classes of burst identified in this study. They occur during the same time intervals during which Minibursts are present. In both of these outbursts, the region of Normal and Minibursts corresponds to the time between the peak of the outburst and the time that the persistent intensity falls below ∼0.1 Crab.

[9]This number does not include Structured Bursts as their complex structure makes them difficult to separate.

Downloaded from https://academic.oup.com/mnras/article-abstract/481/2/2273/5086081 by INAF Brera Milano (Osservatorio Astronomico di Brera) user on 20 February 2019

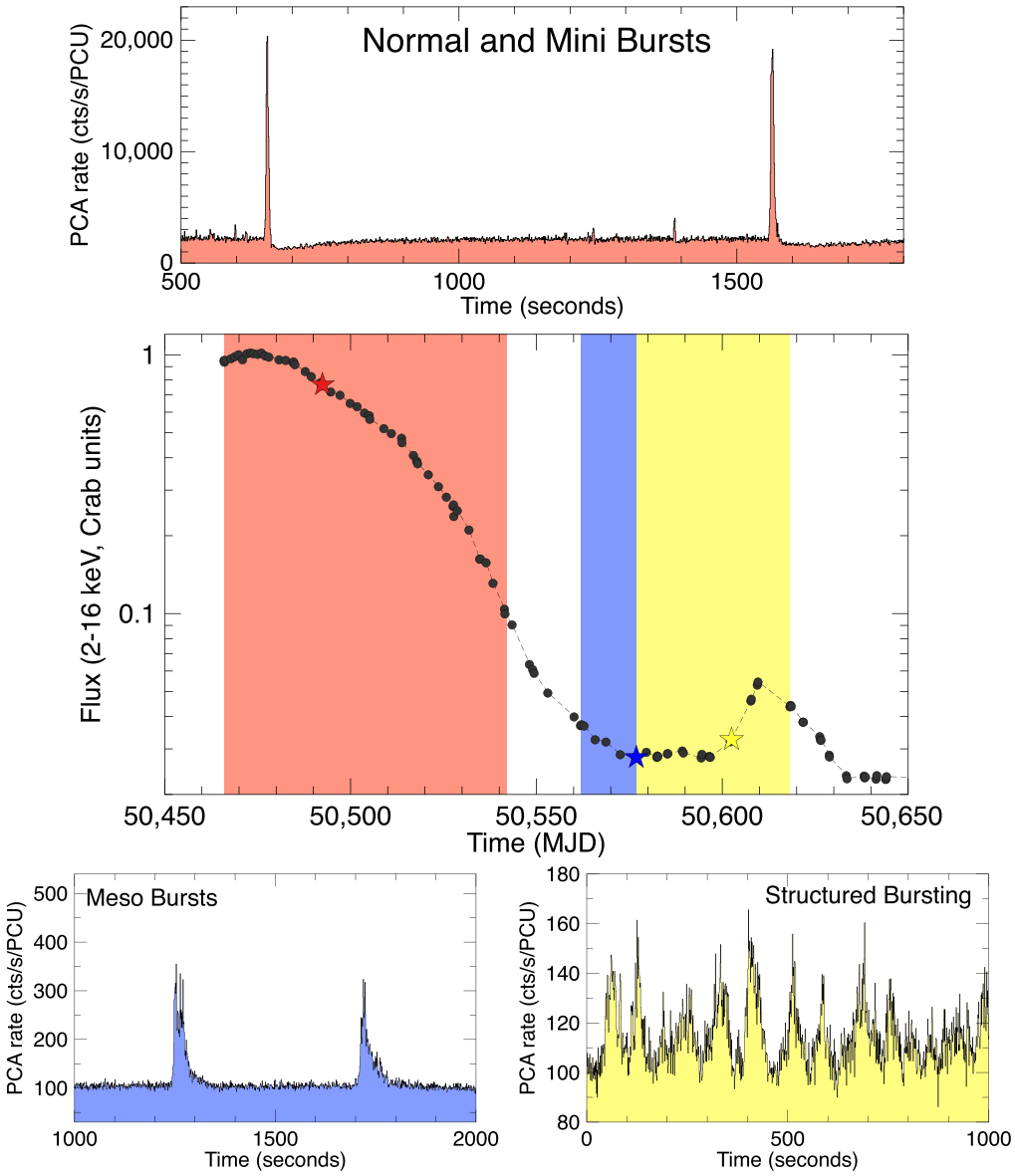

Figure 5. Central panel shows the global 2–16 keV *RXTE*/PCA light curve of the 1997–1999 outburst of the Bursting Pulsar, highlighting periods of time during which Mesobursts (blue), Structured Bursts (yellow), or Normal and Mini bursts (red) are observed. Other panels show example light curves which contain the aforementioned types of bursting behaviour.

Table 3. Statistics on the population of bursts we use for this study, as well as the duration and integrated *RXTE*/PCA exposure time of each mode of bursting. All numbers are the sum of values for Outbursts 1 and 2. As Normal and Minibursts happen during the same period of time in each outburst, the exposure time and mode duration for these classes of bursting are equal.

Bursting Mode	Bursts	Total Exposure (ks)	Duration (d)
Normal Bursts	99	192	76
Minibursts	48	192	76
Mesobursts	43	44	25
Structured Bursts	–	80	54

3.3.1 Recurrence time

Using Outburst 3 data from *Chandra*, *XMM–Newton*, *NuSTAR*, and *Suzaku*, we find minimum and maximum recurrence times of ∼345 and ∼5660 s, respectively.[10] We show the histogram of recurrence times from Outburst 3 in Fig. 6, showing which parts of the distribution were observed with which observatory. Compared to data from *Chandra* and *XMM–Newton*, data from *Suzaku* generally suggests shorter recurrence times. This is likely due to *Suzaku* observations consisting of a number of ∼2 ks windows; as this number is of the

[10]To avoid double-counting peak pairs, we do not use *NuSTAR* observation 80002017004, which was taken simultaneously with *Chandra* observation 16596.

Downloaded from https://academic.oup.com/mnras/article-abstract/481/2/2273/5086081 by INAF Brera Milano (Osservatorio Astronomico di Brera) user on 20 February 2019

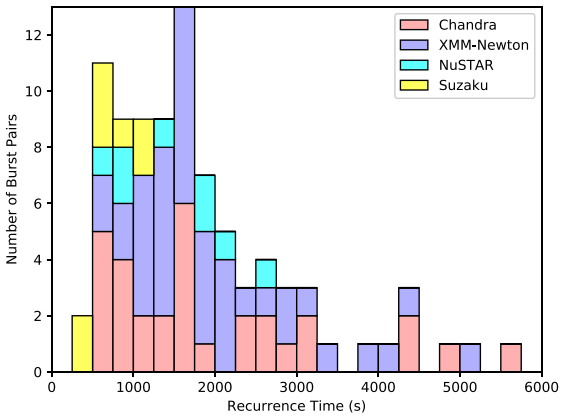

Figure 6. The distribution of recurrence times between consecutive Normal Bursts seen in pointed *Chandra*, *XMM–Newton*, *NuSTAR*, and *Suzaku* observations of Outburst 3 of the Bursting Pulsar. Distributions of bursts observed by different instruments are stacked on top of each other and colour coded.

same order of magnitude as the recurrence time between bursts, there is a strong selection effect against high recurrence times in the *Suzaku* data set.

From the *RXTE* data, we find minimum and maximum burst recurrence times of ∼250 and ∼2510 s during Outburst 1, and minimum and maximum recurrence times of ∼250 and ∼2340 s during Outburst 2. As the length of an *RXTE* pointing ($\lesssim$3 ks) is also of the same order of magnitude as the recurrence time between bursts, selection effects bias us against sampling pairs of bursts with longer recurrence times, and hence this upper value is likely an underestimate.

To test whether consecutive bursts are independent events, we tested the hypothesis that bursts are randomly distributed in time in a Poisson distribution (Poisson 1837). Assuming our hypothesis, as well as assuming that the frequency of Normal Bursts does not change during an outburst (e.g. Aptekar et al. 1998), we could concatenate different observations and the resultant distribution of burst times will still be Poissonian. For each of Outbursts 1 and 2, we concatenated all *RXTE* data during the Normal Bursting part of the outburst into a single light curve. We split our light curves into windows of length w and counted how many bursts were in each, forming a histogram of number of bursts per window. We fit this histogram with a Poisson probability density function, obtaining the value λ which is the mean number of bursts in a time w. λ/w is therefore an expression of the true burst frequency per unit time, and should be independent of our choice of w. We tried values of w between 100 and 10000 s for both outbursts, and found that in all cases λ/w depends strongly on w. Therefore, our assumptions cannot both be valid, and we rejected the hypothesis that these bursts are from a Poisson distribution with constant λ. This in turn suggests at least one of the following must be correct:

(i) The average recurrence time of bursts was not constant throughout the outburst;
(ii) or the arrival time of a given burst depends on the arrival time of the preceding burst, and therefore bursts are not independent events.

3.3.2 *Burst structure*

In the top panel of Fig. 7 we show a plot of all Normal Bursts observed with *RXTE* overlaid on top of one another. We find that

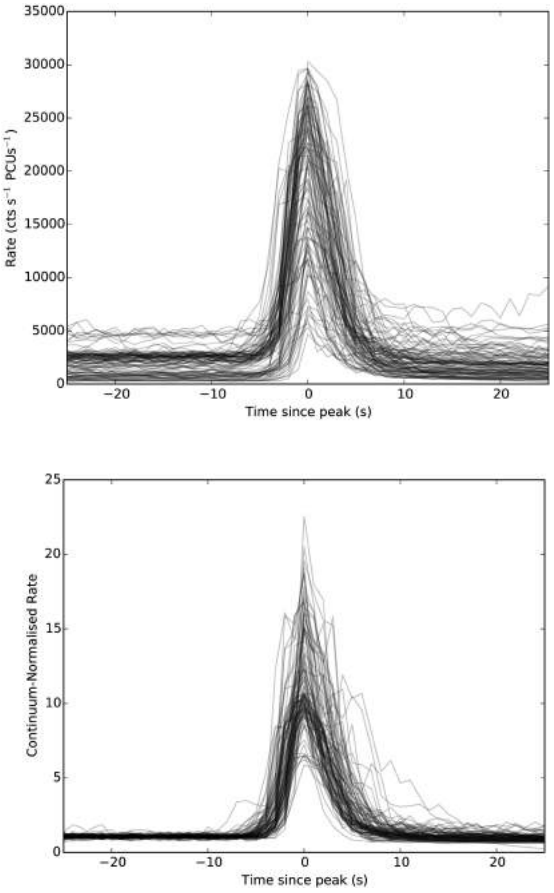

Figure 7. Top: a plot of every Normal Burst, centred by the time of its peak, overlaid on top of each other to show the existence of a common pulse profile. Bottom: a plot of every Normal Burst in which count rates have been normalized by the persistent emission count rate during the observation from which each burst was observed. As the bursts are on average closer to the average pulse profile in this metric, this suggests that the intensity of a burst is roughly dependent on the persistent emission rate. Some persistent emission-normalized count rates may be artificially low due to dead-time effects.

all Normal Bursts follow a similar burst profile with similar rise and decay time-scales but varying peak intensities. In the lower panel of Fig. 7, we show a plot of Normal Bursts overlaid on top of each other after being normalized by the persistent emission count rate in their respective observation. The bursts are even closer to following a single profile in this figure, suggesting a correlation between persistent emission level in an outburst and the individual fluence of its bursts.

The structure of the light curve of a Normal Burst can be described in three well-defined parts:

(i) The main burst: roughly approximated by a skewed Gaussian (see e.g. Azzalini 1985).
(ii) A 'plateau': a period of time after the main burst during which count rate remains relatively stable at a level above the pre-burst rate.
(iii) A 'dip': a period during which the count rate falls below the persistent level, before exponentially decaying back up towards the pre-burst level (e.g. Younes et al. 2015).

The dip is present after every burst in our *RXTE* sample from Outbursts 1 and 2, whereas the plateau is only seen in 39 out

Downloaded from https://academic.oup.com/mnras/article-abstract/481/2/2273/5086081 by INAF Brera Milano (Osservatorio Astronomico di Brera) user on 20 February 2019

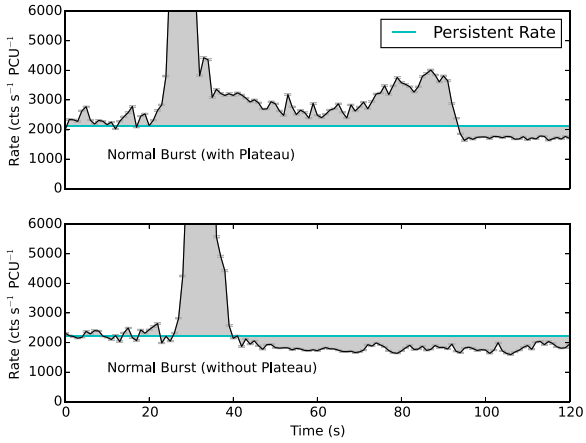

Figure 8. *RXTE* light curves of Normal Bursts with (top) and without (bottom) 'plateau' features, showing the burst structure in each case. The median count rate, which we use as a proxy for the persistent emission, is plotted in cyan to highlight the presence of the count rate 'dip' after each burst.

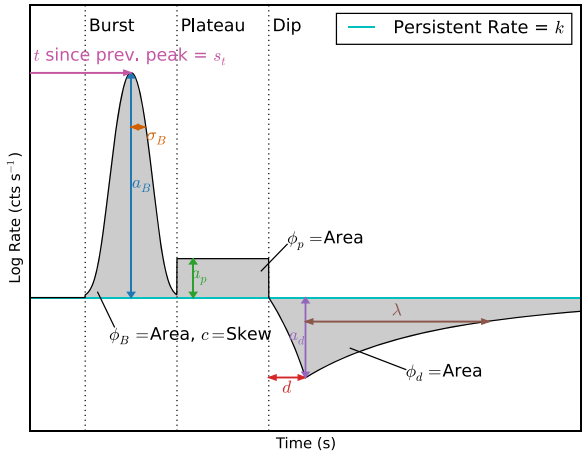

Figure 9. A schematic explaining the origin of the 12 Normal Burst parameters used in this study, as well as showing the functional forms of both the skewed Gaussian fit to a burst and the 'dipper function' (Equation 2) fit to a dip. Note that we do not fit a function to the plateau, and we calculate its fluence by summing the persistent rate-subtracted counts. Diagram is for explanation only and the burst pictured is neither based on real data nor to scale.

of 99. We show example light curves of bursts with and without plateaus in Fig. 8, which also show that the dip is present in both cases.

In order to study Normal Bursts, we fit the burst profiles with phenomenologically motivated mathematical functions. In Fig. 9, we show a schematic plot of our model, as well as annotations explaining the identities of the various parameters we use. We fit the main burst with a skewed Gaussian, centred at $t = x_0$ with amplitude a_b, standard deviation σ_B and skewness[11] c, added to the persistent emission rate k. We fit the 'dip' with the continuous

[11] A measure of how far the peak of the Gaussian is displaced from its centre.

Table 4. A table showing the mean and the standard deviation of 10 Normal Burst parameters of *RXTE*-sampled bursts. In each case, we give the values for populations from only Outburst 1, from only Outburst 2, and from the combined population from both outbursts. Histograms for each parameter can be found in Appendix B.

	Outburst 1		Outburst 2		Outbursts 1 and 2	
	Mean	SD	Mean	SD	Mean	SD
ϕ_B	2.74e6	7.8e5	2.25e6	7.6e5	2.43e6	8.0e5
a_B	3.18e5	8.4e4	2.72e5	9.9e4	2.90e5	9.6e4
σ_B	3.39	0.35	3.42	0.59	3.41	0.52
c	2.68	1.9	2.79	2.0	2.75	2.0
ϕ_d	1.74e6	1.3e6	1.17e6	3.6e5	1.38e6	8.7e5
a_d	550	335	536	307	541	318
d	49	46	20	22	31	36
λ	294	176	229	124	254	150
ϕ_p	1.89e5	2.3e5	7577	5707	1.4e5	1.8e5
a_p	1289	1113	767	463	1063	928

piecewise function $f(t)$:

$$f(t) = \begin{cases} k - \frac{a_d(t-t_0)}{d-t_0}, & \text{if } t \leq d \\ k - a_d \exp\left(\frac{d-t}{\lambda}\right), & \text{otherwise} \end{cases} \quad (2)$$

Where t is time, t_0 is the start time of the dip, a_d is the amplitude of the dip, d is the time at the local dip minimum, and λ is the dip recovery time-scale. This function is based on the finding by Younes et al. (2015) that dip count rates recover exponentially, but has the added advantage that the start of the recovery phase can also be fit as an independent parameter. Using this fit, we can estimate values for burst fluence ϕ_B, burst scale length σ_B, 'missing' dip fluence ϕ_D and dip scale length λ and compare these with other burst parameters. When present, we also calculate the fluence of the plateau ϕ_p by summing the persistent emission-subtracted counts during the region between the end of the burst (as defined in Section 2.1.2) and the start of the dip. For each pair of parameters, we do not consider data points when the magnitude of the error on a parameter is greater than the value of the parameter.

We only extract these parameters from Normal Bursts observed by *RXTE* during Outbursts 1 and 2. This ensures that the resultant parameter distributions we extracted are not affected by differences between instruments.

3.3.3 *Parameter distributions*

We extracted a total of 10 parameters from our fit to each burst: the parameters a_d, d, and λ of the fit to the dip, the missing fluence ϕ_D of the dip, the parameters a_b, σ_B and c of the skewed Gaussian fit to the main burst, the main burst fluence ϕ_B, the maximum persistent emission-subtracted rate in the plateau a_p, and the plateau fluence ϕ_P.

Using our *RXTE* sample of Normal Bursts, we can construct distributions for all of the burst parameters described in Section 3.3.2 for bursts in Outbursts 1 and 2. We give the mean and the standard deviation for each parameter in each outburst in Table 4, and histograms for each can be found in Appendix B.

The mean value of most parameters differs by no more than ~50 per cent between outbursts. Notable exceptions are d, ϕ_p, ϕ_d, and a_p, which are ~2.5, ~2.5 ~1.5, and ~1.7 times greater in

Downloaded from https://academic.oup.com/mnras/article-abstract/481/2/2273/5086081 by INAF Brera Milano (Osservatorio Astronomico di Brera) user on 20 February 2019

Outburst 1 than in Outburst 2, respectively. The less significant differences between values of ϕ_B and a_B in Outbursts 1 and 2 are expected, as the amplitude of a burst correlates with k which was generally higher in Outburst 1 than in Outburst 2.

3.3.4 Correlations

In total, we extracted 12 parameters for each Normal Burst in our *RXTE* sample: the 10 burst parameters listed in Section 3.3.3, the recurrence time s_t until the next burst, and the persistent emission rate k at the time of the burst.

As the amplitude of all three components in a burst scale with the persistent level, we rescaled our values of a_b, a_d, ϕ_B, ϕ_D, and ϕ_P by a factor $\frac{1}{k}$. We show the covariance matrix with all 66 possible pairings of these normalized parameters in Fig. 10 (we present the covariance matrix of these parameters before being rescaled in Appendix C). Using the Spearman's Rank Correlation Coefficient, we find the following $\geq 5\,\sigma$ correlations which are highlighted in Fig. 10:

(i) Persistent emission k anticorrelates with normalized burst fluence ϕ_B/k ($>10\,\sigma$) and normalized burst amplitude a_b/k ($>10\,\sigma$).
(ii) Normalized burst fluence ϕ_B/k correlates with normalized burst amplitude a_B/k ($8.0\,\sigma$).
(iii) Normalized dip fluence ϕ_d/k correlates with dip recovery time-scale λ ($6.3\,\sigma$).
(iv) Normalized dip amplitude a_d/k anticorrelates with dip fall time d ($5.7\,\sigma$) and dip recovery time-scale λ ($7.1\,\sigma$).
(v) Normalized plateau fluence ϕ_p/k correlates with normalized plateau amplitude a_p ($6.4\,\sigma$).

As ϕ_B can be approximated to first order as a product of a_B and σ, the correlation between ϕ_B and a_B is expected as they are not independent parameters. Similarly, the correlations between ϕ_d and λ and ϕ_p and a_p are likely due to these pairs of parameters not being independent.

3.3.5 Colour evolution

To explore the spectral behaviour of Normal Bursts, we studied the evolution of the hardness (the ratio between count rate in the energy bands ∼2–7 and ∼8–60 keV energy bands) as a function of count rate during the individual bursts. These 'hardness-intensity diagrams' allow us to check for spectral evolution in a model-independent way. We do not correct them for background as the count rates in both bands are very high.

We find evidence of hysteretic loops in hardness-intensity space in some, but not all, of the Normal Bursts in our sample; see Fig. 11 for an example of such a loop. The existence of such a loop suggests significant spectral evolution throughout the burst. This finding can be contrasted with results from previous studies in different energy bands (e.g. Woods et al. 1999 from ∼25–100 keV) which suggested no spectral evolution during type II bursts in this source.

3.4 Minibursts

We define Minibursts as the set of all bursts with a peak 1 s binned *RXTE*/PCA-equivalent count rate of $<$ 300 per cent of the persistent rate. Minibursts account for 48 out of the 190 bursts identified for this study. They are observed during all three outbursts, and occur during the same times that Normal Bursts are present. Minibursts occurred between MJDs 50117 and 50200 in Outburst 1, and between 50466 and 50542 in Outburst 2; during these intervals, *RXTE* observed the source for a total of 192 ks. These intervals correspond to the times between the peak of each outburst and the time that the persistent intensity falls below ∼0.1 Crab.

3.4.1 Recurrence time

There are only 10 observations with *RXTE* which contain multiple Minibursts. Using these, we find minimum and maximum Miniburst recurrence times of 116 and 1230 s.

We find 17 *RXTE* observations which contain both a Miniburst with a preceding Normal Burst, and find minimum and maximum Normal Burst → Miniburst recurrence times of 461 and 1801 s.

3.4.2 Structure

In Fig. 12, we show a representative Miniburst, and we show all Minibursts overplotted on each other in Fig. 13. These bursts are roughly Gaussian in shape with a large variation in peak count rate; as can be seen in Fig. 13, however, the persistent-normalized peak count rates of Minibursts are all roughly consistent with 2.

Minibursts are all ∼5 s in duration, and some show signs of a 'dip' feature similar to those seen in Normal Bursts. We find that the time-scales of these dips are all $\lesssim$10 s. We estimate 'missing' fluence in each dip by integrating the total persistent-rate-subtracted counts between the end of the burst and a point 10 s later. If this 'missing fluence' is less than half of the standard deviation in count rate multiplied by 5 s, which represents the smallest $<$10 s triangle-shaped dip which would be detectable above noise in a given data set, we treat the dip in that outburst as not being detected.

Due to the relatively short duration and low peak count rates of Minibursts, we are unable to reliably discern whether they contain a single peak or multiple peaks. For this reason, we also do not fit them mathematically.

3.4.3 Parameters and correlations

For each Miniburst, we are able to extract the same parameters that we extracted from Mesobursts (see list in Section 3.5.3). The mean and the standard deviation of each of these parameters, calculated from *RXTE* data, are presented in Table 5 for Outburst 1, Outburst 2, and the combined population of Minibursts from Outbursts 1 and 2. The standard deviations on the fluence and peak rates of Minibursts are very large, suggesting that these parameters are distributed broadly.

Using the Spearman's Rank metric, we find only two correlations above the $5\,\sigma$ level:

(i) Fluence is correlated with peak rate ($7.3\,\sigma$).
(ii) Fluence divided by persistent rate is correlated with peak rate divided by persistent rate ($7.1\,\sigma$).

As in Normal Bursts, a correlation between peak rate and fluence is to be expected. However, due to the poor statistics associated with Miniburst parameters, it is likely that other parameter pairs are also correlated.

3.4.4 Colour evolution

Minibursts show the greatest magnitude of evolution in colour of all the classes of burst. In Fig. 14, we show how the hardness ratio

Downloaded from https://academic.oup.com/mnras/article-abstract/481/2/2273/5086081 by INAF Brera Milano (Osservatorio Astronomico di Brera) user on 20 February 2019

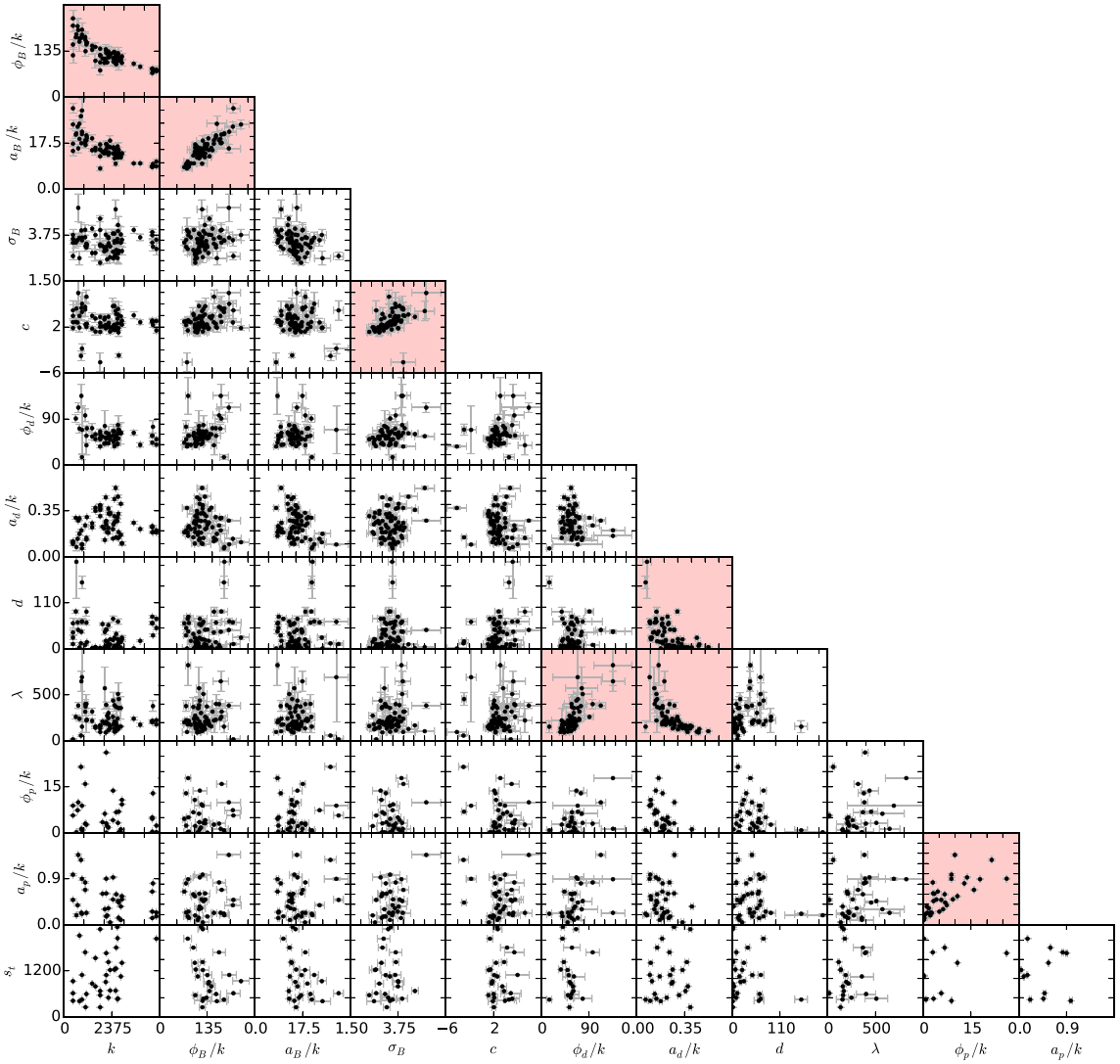

Figure 10. Covariance Matrix with a scatter plot of each of the 66 pairings of the 12 Normal Burst parameters listed in Section 3.3.4. Amplitudes and fluences have been normalized by dividing by the persistent count rate k. Pairings which show a correlation using the Spearman Rank metric with a significance $\geq 5\,\sigma$ are highlighted in red.

between the 4–10 and 2–4 keV energy bands changes during an observation containing both a Miniburst and a Normal Burst. We find that the hardness ratio increases by ∼50 per cent in a Miniburst, significantly more than the change in hardness during Normal or Mesobursts. The statistics in minibursts were too poor to check for the presence of hysteresis.

3.5 Mesobursts

We define Mesobursts as the set of all bursts with a persistent-emission-subtracted peak 1 s binned *RXTE*/PCA-equivalent count rate below 3000 cts s^{-1} PCU^{-1} in which the peak of the burst reaches at least 300 per cent of the persistent rate. Mesobursts account for 43 out of the 190 bursts identified for this study. They are observed in *RXTE* data from both Outbursts 1 and 2; in both cases they occur after the main outburst and before or during a rebrightening event. Mesobursts occurred between MJDs 50238 and 50248 in Outburst 1, and between 50562 and 50577 in Outburst 2; during these intervals, *RXTE* observed the source for a total of 44 ks. As no soft X-ray instrument monitored the Bursting Pulsar during the latter stages of Outburst 3, it is unclear whether Mesobursts occurred during this outburst. The one pointed observation of *NuSTAR* made during this time did not detect any Mesobursts.

3.5.1 Recurrence time

Only six *RXTE* observations in Outburst 1, and four in Outburst 2, contain multiple Mesobursts. From our limited sample, we find minimum and maximum recurrence times of ∼230 and ∼1550 s in Outburst 1 and minimum and maximum recurrence times of ∼310 and ∼2280 s in Outburst 2.

3.5.2 Structure

The structure of the main part of a Mesoburst is significantly more complex than in Normal Bursts, consisting of a large number of secondary peaks near the main peak of the burst. Mesobursts never show the post-burst ‘dip’ feature that we see in Normal Bursts, but

Downloaded from https://academic.oup.com/mnras/article-abstract/481/2/2273/5086081 by INAF Brera Milano (Osservatorio Astronomico di Brera) user on 20 February 2019

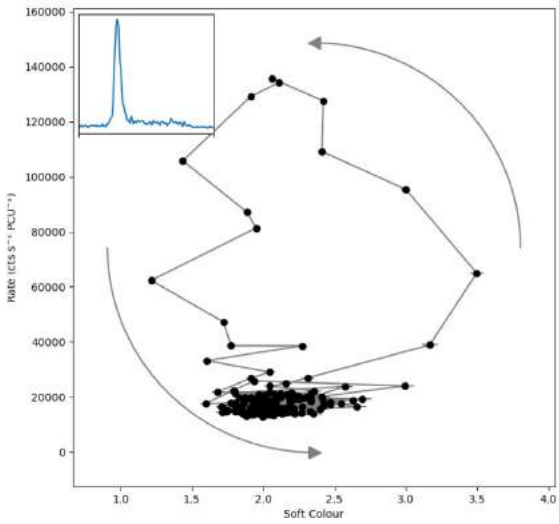

Figure 11. A 1 s-binned hardness-intensity diagram of a Normal Burst from *RXTE*/PCA observation 10401-01-08-00, with an inset 2–60 keV light curve. Significant colour evolution can be seen during the burst, taking the form of a loop.

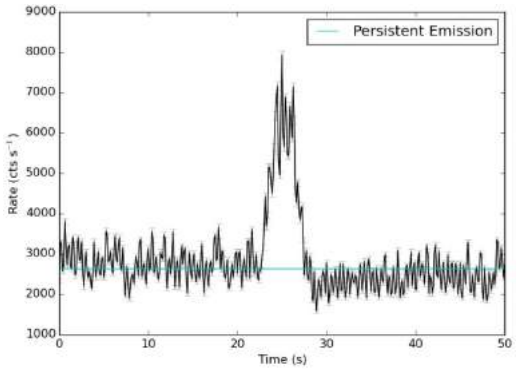

Figure 12. A representative *RXTE* light curve of a Miniburst from OBSID 20077-01-03-00 in Outburst 2.

they can show 'plateaus'. In Fig. 15, we show an example of a Mesoburst with a plateau similar to those seen after Normal Bursts, suggesting a connection between the two classes.

In Fig. 16, we show the plot of all Mesobursts observed by *RXTE* overlaid on top of each other before (top panel) and after (bottom panel) being renormalized by persistent emission rate. It can be seen that the intensity and structure of these bursts is much more variable than in Normal Bursts (see Fig. 7). However, each Mesoburst has a fast rise followed by a slow decay, and they occur over similar time-scales of ∼10–30 s.

3.5.3 Parameters and correlations

Due to the complexity structure of Mesobursts, we do not fit them mathematically as we did for Normal Bursts. Instead, we define a number of different parameters for each Mesoburst, listed below:

(i) Total burst fluence and burst fluence divided by persistent emission.

(ii) Peak 1 s binned rate and peak rate divided by persistent emission.

(iii) Rise time, fall time, and total time.

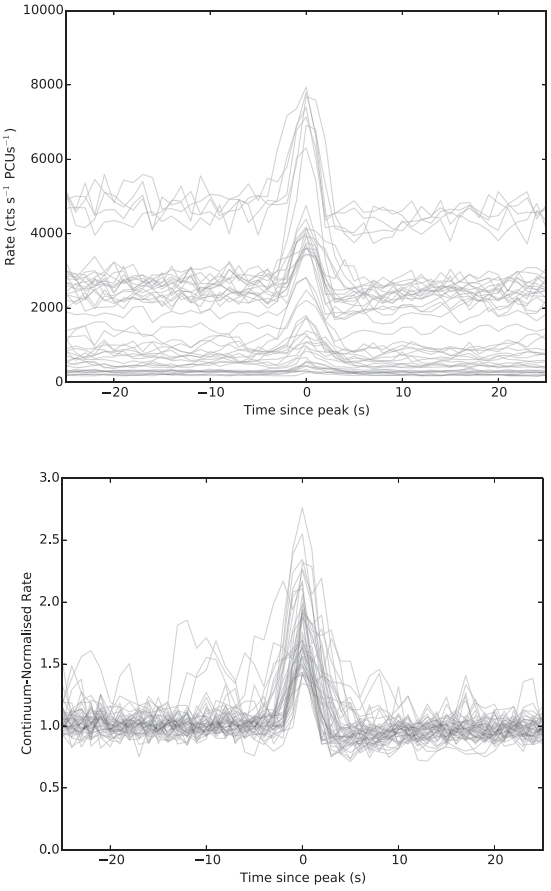

Figure 13. Top: a plot of every Miniburst, centred by the time of its peak, overlaid on top of each other. Bottom: a plot of every Miniburst in which count rates have been normalized by the persistent emission count rate during the observation from which each burst was observed.

Table 5. A table showing the mean and the standard deviation of seven parameters of *RXTE*-sampled Minibursts from Outburst 1, Outburst 2, and both outbursts combined. Fluence is given in cts PCU^{-1}, peak rate is given in cts s^{-1} PCU^{-1}, and rise, fall, and total time are given in s. k is the persistent emission rate during the observation in which a given burst was detected.

	Outburst 1		Outburst 2		Outbursts 1 and 2	
	Mean	SD	Mean	SD	Mean	SD
Fluence	6792	5776	4474	3307	5422	4627
Peak rate	3501	2851	2473	1664	2902	2293
Fluence/k	3.67	1.13	3.58	1.47	3.61	1.34
Peak rate/k	1.90	0.37	1.76	0.28	1.82	0.32
Rise time	2.33	0.8	2.03	1.1	2.15	1.0
Fall time	2.32	0.9	2.35	1.0	2.32	0.9
Tot. time	4.61	1.0	4.38	01.0	4.47	1.0

The mean and the standard deviation of each of these parameters, calculated from *RXTE* data, are presented in Table 6. Due to the relative low number of Mesobursts compared to Normal Bursts, we only present the results from the combined set of bursts in both Outbursts 1 and 2. In general, Mesobursts are longer in duration than Normal Bursts, and have significantly smaller amplitudes and fluences (compare e.g. Table 4).

Downloaded from https://academic.oup.com/mnras/article-abstract/481/2/2273/5086081 by INAF Brera Milano (Osservatorio Astronomico di Brera) user on 20 February 2019

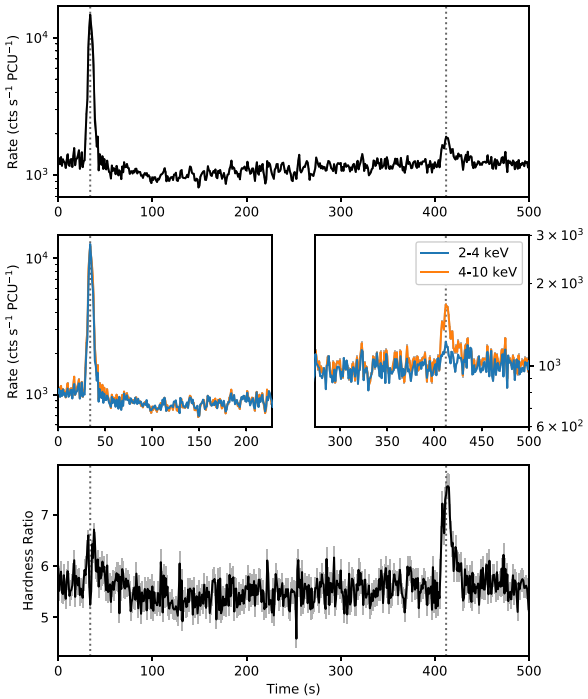

Figure 14. A portion of observation 10401-01-16-00, featuring a Normal Burst (∼30 s) and a Miniburst (∼410 s). The top panel shows the total 2–10 keV light curve. The middle panel shows light curves from two different energy bands; the count rates from the soft energy band have been multiplied by 5.4 so they can more easily be compared with the hard energy band. The bottom panel shows the evolution over time of the ratio between the rates in the two bands. As can be seen in panels 2 and 3, the Miniburst has a significantly higher fractional amplitude in the 4–10 keV energy band than in the 2–4 keV band.

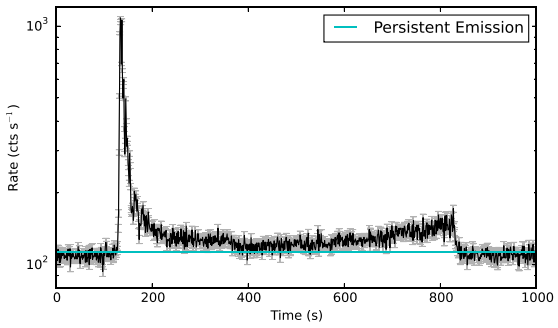

Figure 15. A light curve from *RXTE* observation 20078-01-17-00 from Outburst 2, showing an apparent 'plateau' feature after a Mesoburst.

Using the Spearman's Rank metric, we find a number correlations above the 5 σ level:

(i) Fluence is correlated with peak rate (>10 σ), peak rate divided by persistent rate (6.7 σ), fall time (6.8 σ), total time (6.0 σ).
(ii) Fluence divided by persistent rate is correlated with peak rate divided by persistent rate (7.3 σ).
(iii) Peak rate is also correlated with peak rate divided by persistent rate (7.4 σ), fall time (5.8 σ), and persistent level (6.2 σ).
(iv) Rise time correlates with total time (5.4 σ).
(v) Fall time correlates with total time (>10 σ).

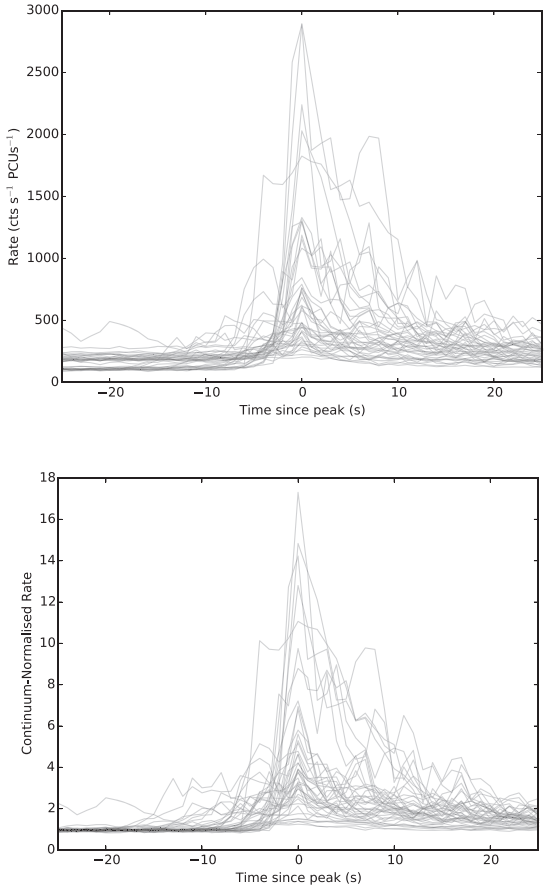

Figure 16. Top: a plot of every Mesoburst, centred by the time of its peak, overlaid on top of each other. Bottom: a plot of every Mesoburst in which count rates have been normalized by the persistent emission count rate during the observation from which each burst was observed.

Table 6. A table showing the mean and the standard deviation of seven burst parameters of *RXTE*-sampled Mesobursts from Outbursts 1 and 2. k is the persistent emission rate during the observation in which a given burst was detected.

	Mean	Standard deviation
Fluence (cts PCU^{-1})	6067	6707
Peak rate (cts s^{-1} PCU^{-1})	665.4	658.4
Fluence/k	48.6	32.8
Peak rate/k	5.32	4.0
Rise time (s)	6.95	4.9
Fall time (s)	18.28	10.8
Total time (s)	25.88	13.3

Again, the correlation between fluence and peak rate is expected, as is the correlation between peak rate and peak rate divided by persistent rate.

3.5.4 *Colour evolution*

The hardness ratio of the emission from the source decreases significantly during Mesobursts, with the PCA 8–60/2–7 keV colour decreases from ∼0.6 between bursts to ∼0.2 at the peak of a burst. Due to the poor statistics of these features compared with Normal Bursts, we were unable to check for evidence of hardness-intensity hysteresis.

Downloaded from https://academic.oup.com/mnras/article-abstract/481/2/2273/5086081 by INAF Brera Milano (Osservatorio Astronomico di Brera) user on 20 February 2019

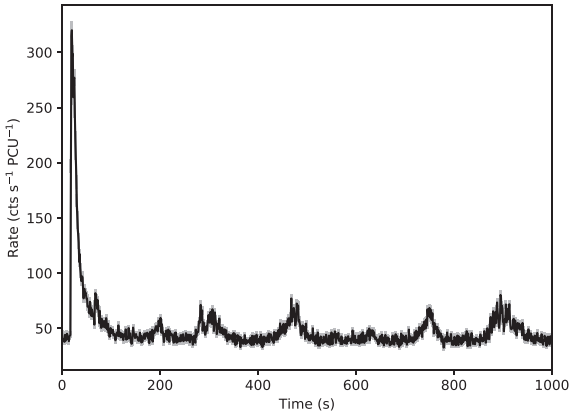

Figure 17. A light curve from *RXTE*/PCA observation 10401-01-57-03, showing a Mesoburst occurring during a period of Structured Bursting.

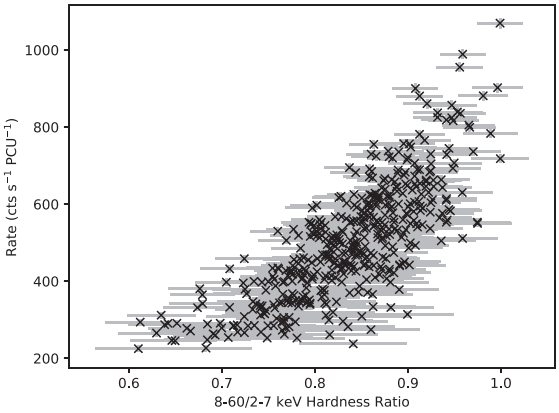

Figure 18. A 1 s-binned hardness-intensity diagram from *RXTE* observation 20078-01-23-00, showing that hardness tends to correlate with intensity during Structured Bursting. Data are binned to 8 s, and background has been estimated by subtracting mean count rates in the relevant energy bands from *RXTE* OBSID 30075-01-26-00.

3.6 Structured 'Bursts'

We define Structured Burst observations as observations in which the recurrence time between bursts is less than, or approximately the same as, the duration of a single burst. Structured Bursts constitute the most complex behaviour we find in our data set. Unlike the other classes of burst we identify, Structured Bursts are not easily described as discrete phenomena. We find Structured Bursts in 54 observations which are listed in Appendix A.

In both outbursts covered by *RXTE*, Structured Bursts occur in the time between the end of the main outburst and the start of a rebrightening event. In both cases, these periods of structured outbursts are preceded by a period populated by Mesobursts. Mesobursts occurred between MJDs 50248 and 50261 in Outburst 1, and between 50577 and 50618 in Outburst 2; during these intervals, *RXTE* observed the source for a total of 81 ks. Notably, as we show in Fig. 17, one Outburst 1 *RXTE* light curve containing Structured Bursting also contains a bright Mesoburst.

In both outbursts, the amplitude of Structured Bursting behaviour decreases as the outburst approaches the peak of the rebrightening event. This amplitude continues to decrease as the Structured Burst behaviour evolves into the low-amplitude noisy behaviour associated with the source's evolution towards the hard state.

3.6.1 Colour evolution

We produce hardness-intensity diagrams for a number of Structured Burst observations; we show a representative example in Fig. 18. We find that hardness is strongly correlated with count rate during this class of bursting, but that the magnitude of the change in hardness is no greater than ∼30 per cent. This is less than the change in hardness that we see during Normal or Minibursts. We also find no evidence of hysteretic hardness-intensity loops from Structured Bursts.

3.6.2 Types of Structured Bursting

In Fig. 19, we present a selection of light curves which show the different types of variability that can be seen during periods of Structured Bursting. These consist of a variety of patterns of peaks and flat-bottomed dips, and both *RXTE*-observed outbursts show several of these different patterns of Structured Bursting. As all types of Structured Bursting have similar amplitudes and occur in the same part of each outburst, we consider them to be generated by the same physical process. We do not separate these patterns into separate subclasses in this paper.

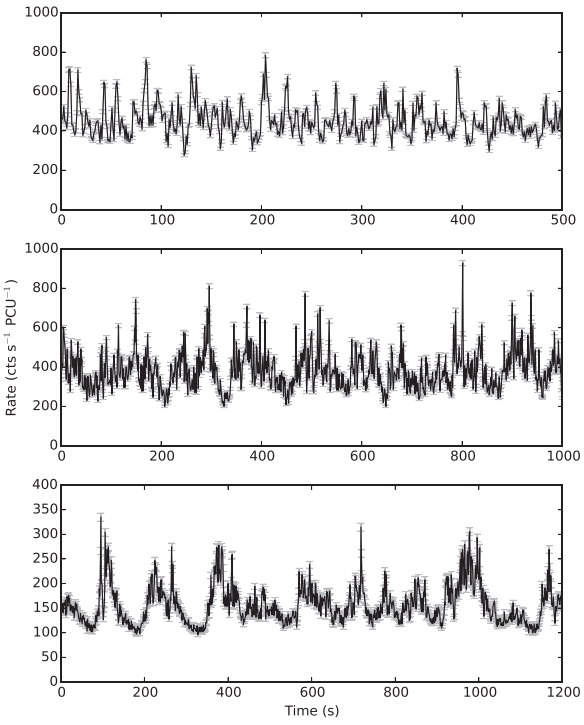

Figure 19. A selection of *RXTE* light curves from Structured Bursting observations of the Bursting Pulsar. Top: a light curve from Outburst 1 showing flaring on time-scales of ∼10 s. Middle: a light curve from Outburst 1 showing the same flaring behaviour with an additional slower modulation over ∼50 s. Bottom: a light curve from Outburst 2 showing a regular sequence of flat-bottomed dips and multipeaked flaring. These show the wide variety of variability patterns that we classify as 'Structured Bursting'.

4 DISCUSSION

We analyse all available X-ray data from the first three outbursts of the Bursting Pulsar. The bursting behaviour evolves in a similar way during these outbursts, strongly associating them with the Bursting

Downloaded from https://academic.oup.com/mnras/article-abstract/481/2/2273/5086081 by INAF Brera Milano (Osservatorio Astronomico di Brera) user on 20 February 2019

Pulsar and suggesting an underlying connection between the classes of burst. We also find that both Outbursts 1 and 2 showed 'rebrightening events' similar to those seen in a number of other LMXBs as well as in dwarf novae (e.g. Wijnands et al. 2001; Patruno et al. 2016)

We find that the type II X-ray bursts from these data can be best described as belonging to four phenomenological classes: Normal Bursts, Minibursts, Mesobursts, and Structured Bursts. For each of these four classes, we collect a number of statistics to shed light on the physical mechanisms that generate these light-curve features.

Normal Bursts and Minibursts both represent the 'type II' bursting behaviour which is observed most commonly from this source. Mesobursts occur much later on in the outburst and show fast-rise slow-decay profiles; they are generally much fainter and more structured than Normal Bursts. Finally, Structured Bursts form continuous highly structured regions of bursting over time-scales of days. All Normal Bursts and some Minibursts show count rate 'dips' after the main burst, while Mesobursts and Structured Bursts do not. In addition to this, some Normal and Mesobursts show count rate 'plateaus'; regions of roughly stable count rate above the persistent level which last for tens of seconds. These features are also sometimes seen in Mesobursts, while Minibursts and Structured Bursts never show these structures.

Here, we discuss these results in the context of models proposed to explain type II bursting. We also compare our results with those of previous studies on bursting in both the Bursting Pulsar and the Rapid Burster.

4.1 Evolution of outburst and bursting behaviour

In general, Outburst 1 was brighter than Outburst 2, with the former having a peak 2–60 keV intensity a factor of ∼1.7 greater than the latter. However, in Fig. 1 we show that both outbursts evolve in a similar way. In both outbursts, the intensity of the Bursting Pulsar reaches a peak of order ∼1 Crab before decreasing over the next ∼100 d to a level of a few tens of mCrab. A few tens of days after reaching this level, the light curves of both outbursts show a pronounced 'rebrightening' event, during which the intensity increases to ∼100 mCrab for ∼10 d. Outburst 1 shows a second rebrightening event ∼50 d after the first. It is unclear whether any rebrightening events occurred in Outburst 3 due to a lack of late-time observations with soft X-ray telescopes. X-ray 'rebrightening' events have been seen after the outbursts of a number of other LMXBs with both neutron star and black hole primaries: including SAX J1808.4–3658 (Wijnands et al. 2001), XTE J1650–500 (Tomsick et al. 2003), and IGR J17091–3625 (Court et al. 2017).

As we have shown in Figs 4 and 5, the nature of bursts from the Bursting Pulsar evolves in a similar way in both Outbursts 1 and 2. Starting from around the peak of each outburst, both Normal and Minibursts are observed. The fluence of these bursts decreases over time as the X-ray intensity of the source decreases, before bursting shuts off entirely when the 2–16 keV flux falls below ∼0.1 Crab. After a few tens of days with no bursts, bursting switches back on in the form of Mesobursts; this occurs during the tail of a rebrightening event in Outburst 1, but in the tail of the main outburst in Outburst 2. Mesobursting continues until the 2–16 keV source flux falls below ∼0.03 Crab, at which point we observe the onset of Structured Bursting. In both Outbursts, Structured Bursting stops being visible a few tens of days later during the start of a rebrightening event. Because this evolution is common to both of the outbursts observed by *RXTE*, this strongly indicates that the nature of bursting in the Bursting Pulsar is connected with the evolution of its outbursts. Additionally, with the exceptions of Normal and Minibursts, we show that each class of burst is mostly found in a distinct part of the outburst corresponding to a different level of persistent emission.

In Fig. 20, we show light curves from Outburst 2 taken a few days before and after the transition from Mesobursts to Structured Bursting. We can see that, as the system approaches this transition, Mesobursts become more frequent and decrease in amplitude. Additionally, in Fig. 17 we show a light curve which contains both a Mesoburst and Structured Bursting. We find that, instead of a well-defined transition between these bursting classes, there is a more gradual change as Mesobursting evolves into Structured Bursting. This suggests that the same mechanism is likely to be responsible for both of these types of burst.

The transition between Normal Bursts and Mesobursts, however, is not smooth; in both outbursts these two classes of bursting are separated by ∼10 d gaps in which no bursts of any kind were observed at all. If all our classes of burst are caused by the same or similar processes, any model to explain them will also have to explain these periods with no bursts.

4.2 Parameter correlations

We extracted a number of phenomenological parameters from each Normal Burst, Miniburst, and Mesoburst. For Normal Bursts, we extracted a large number of parameters by fitting a phenomenological model described in Section 3.3.2. For Minibursts and Mesobursts, we extracted recurrence times and persistent emission-subtracted peak rates; we also calculated burst fluences by integrating the persistent emission-subtracted rate over the duration of the burst. We do not extract similar parameters for Structured Bursts due to their complex nature.

In all three of the classes of burst we consider, we found that fluence and peak rate correlate strongly with persistent emission. For each type of burst case, the slope of these correlations is consistent with being equal during Outbursts 1 and 2.

We also compared the Normal Bursts in Outburst 1 with the Normal Bursts in Outburst 2. The only significant statistical differences we found between these two populations were in the burst peak rate and the burst fluence; both of these parameters are generally higher for Normal Bursts in Outburst 1. As both of these parameters strongly depend on the persistent emission, both of these differences can be attributed to the fact that Outburst 1 was significantly brighter at peak than Outburst 2.

For Normal Bursts, we found additional correlations. Of particular note, we found that both the fall time and the recovery time-scale of a 'dip' is proportional to its amplitude, which has implications for the possible mechanism behind these features. We discuss this further in Section 4.5.

These findings strongly suggest that the properties of Normal, Mini, and Mesobursts depend on the persistent luminosity of the Bursting Pulsar. Assuming that this persistent luminosity is proportional to $\dot{M}$, this suggests that all classes of bursting are sensitive to the accretion rate of the system. Additionally, with the exceptions of Normal and Minibursts, we find that each class of burst is mostly found in a distinct part of the outburst corresponding to a different level of persistent emission. We suggest that Normal, Meso, and Structured Bursts may in fact be manifestations of the same physical instability but at different accretion rates. This is supported by the observation of a Mesoburst during a period of Structured Bursting, which we show in the light curve in Fig. 17. This shows that the conditions for both Meso and Structured Bursting can be met at the same time.

Downloaded from https://academic.oup.com/mnras/article-abstract/481/2/2273/5086081 by INAF Brera Milano (Osservatorio Astronomico di Brera) user on 20 February 2019

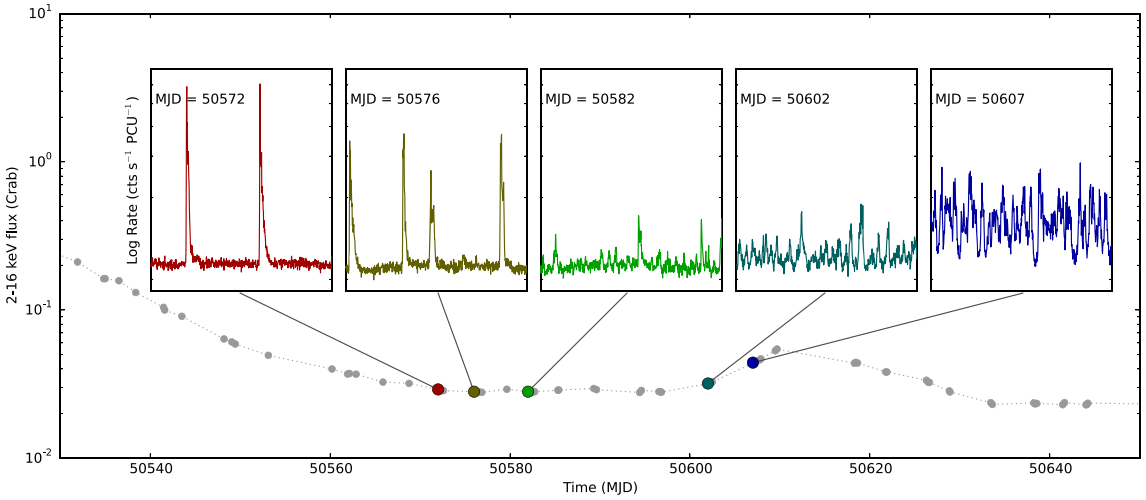

Figure 20. A series of light curves from *RXTE*/PCA observations of Outburst 2, showing a gradual evolution from Mesobursts to Structured Bursting over a period of ∼30 d. Each inset light curve is plotted with the same *y*-scaling, and each corresponds to 2 ks of data.

Table 7. A table showing how our burst classes map to those described in Giles et al. (1996). Giles et al. (1996) do not consider the times during the outburst when Structured Bursts appear, and we consider G_3 bursts described by Giles et al. (1996) to be consistent with flicker noise.

Our class	Giles et al. class
Normal Bursts	G_1
Mesobursts	G_1
Miniburst	G_2
Structured Bursts	–
–	G_3

4.3 Comparison with previous studies

In their study of bursts in the Bursting Pulsar, Giles et al. (1996) found evidence for three distinct classes of type II bursts in the Bursting Pulsar:

(i) 'Bursts' (hereafter G_1 bursts to avoid confusion), the common type II bursts seen from the source.
(ii) 'Minibursts' (hereafter G_2 Bursts), with smaller amplitudes up to ∼2 times the persistent emission level.
(iii) 'Microbursts' (hereafter G_3 Bursts), second-scale bursts with amplitudes of ∼50–100 per cent of the persistent level.

We find that the Giles et al. (1996) G_1 category contains the bursts that we identify as Normal Bursts, while our Miniburst category contains the same bursts as Giles' G_2 category. Giles et al. (1996) only consider bursts up to MJD 50204 in their classification, and they could not classify any bursts that we identify as Mesobursts; under their framework, we find that Mesobursts would also be categorized as G_1. We present the full mapping between Giles classes and our classes in a schematic way in Table 7.

Giles et al. (1996) note the presence of both dips and plateaus in Normal Bursts. To calculate the fluence of each main burst and its associated dip, Giles et al. (1996) integrate the total persistent-emission-subtracted counts in each feature. They calculate that ratio between burst fluence and 'missing' dip fluence (ϕ_B/ϕ_d) is between 0.26 and 0.56 in Outburst 1 before correcting for dead-time effects. Using bursts in which our mathematical fit gave well-constrained ($>5\sigma$) values for both burst and dip fluence, we find that ϕ_B/ϕ_d is between 1.3 and 2.0 in Outburst 1 and between 1.3 and 2.9 in Outburst 2. Our values differ significantly from those reported from Giles et al. (1996); this is likely due to differing definitions of the persistent emission level and the start and end times of each dip, as Giles et al. (1996) do not report how they define these features.

Our values for the ratios between burst and dip fluences, as well as those of Giles et al. (1996), are affected by dead time. These effects cause the fluence of bursts to be underreported, as can be inferred from Fig. 22, but the integrated counts in dips are not significantly affected (Giles et al. 1996). Therefore, correcting for dead time can only increase the value of ϕ_B/ϕ_d, and our result shows that the fluence of a burst is always greater than the fluence 'missing' from a dip.

We find evidence of significant colour evolution during both Normal Bursts and Minibursts, which is strongly indicative of a spectral evolution (see also e.g. Woods et al. 1999). Further work on the time-resolved spectra of this source will likely allow us to better understand the underlying physics of its behaviour.

Using data from the KONUS experiments aboard the GGS-Wind and Kosmos-2326 satellites, Aptekar et al. (1998) have previously found that the recurrence times between consecutive bursts in Outburst 1 are distributed with a constant mean of ∼1776 s. This is substantially longer than our value of 1209 s that we find for Outburst 1, but our value is likely an underestimate due to a selection bias caused by the relatively short pointings of *RXTE*.

Using *Chandra* and *XMM–Newton* data, we find a mean recurrence time for Outburst 3 of 1986 s; as pointings with these instruments are significantly longer than the burst recurrence time-scale, windowing effects are negligible. As this value is close to the value that Aptekar et al. (1998) find for mean recurrence time, our result is consistent with the burst rate in all three outbursts being approximately the same.

Previous studies with *CGRO*/BATSE have found that the burst rate during the first few days of Outbursts 1 and 2 was significantly higher than during the rest of each outburst (Kouveliotou et al. 1996; Woods et al. 1999). As *RXTE* did not observe either of these times, we are unable to test this result.

4.4 Comparison with other objects

In Court, Altamirano & Sanna (2018), we discuss the possibility that some of the behaviour in the Bursting Pulsar could be due to fluctuations in the magnetospheric radius of the system close

Downloaded from https://academic.oup.com/mnras/article-abstract/481/2/2273/5086081 by INAF Brera Milano (Osservatorio Astronomico di Brera) user on 20 February 2019

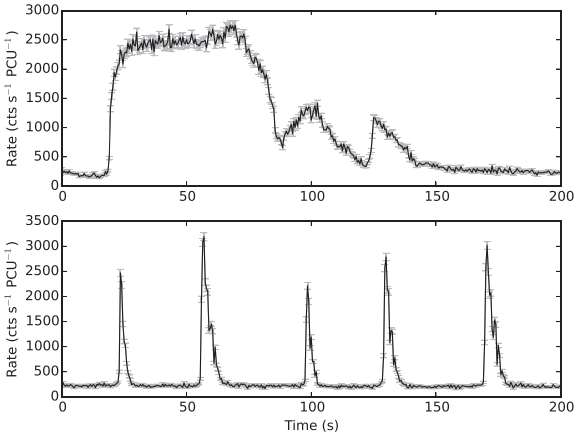

Figure 21. *RXTE* light curves of representative Long (top) and Short (bottom) bursts from the Rapid Burster. These bursts were identified and classified by Bagnoli et al. (2015).

to the corotation radius. This behaviour (e.g. Ferrigno et al. 2014; Bogdanov et al. 2015) is also seen in 'Transitional Millisecond Pulsars' (TMSPs): objects which alternate between appearing as X-ray pulsars and radio pulsars (see e.g. Archibald et al. 2009; Papitto et al. 2013).

Another natural comparison to the Bursting Pulsar is the Rapid Burster (Lewin, Clark & Doty 1976b), a neutron star LMXB in the globular cluster Liller I. This object is the only LMXB other than the Bursting Pulsar known to unambiguously exhibit type II bursting behaviour during outbursts. Rappaport & Joss (1997) have previously proposed that the Bursting Pulsar, the Rapid Burster, and other neutron star LMXBs form a continuum of objects with different magnetic field strengths.

We compare our study of bursts in the Bursting Pulsar with studies of type II bursts in the Rapid Burster, particularly the detailed population study performed by Bagnoli et al. (2015). Bagnoli et al. (2015) found that type II bursting begins during the decay of an outburst in the Rapid Burster. This is the same as what we see in the Bursting Pulsar, where we find Normal Bursting behaviour starts during the outburst decay. Bagnoli et al. (2015) found that all bursting in the Rapid Burster shuts off above an Eddington fraction of $\gtrsim$0.05, whereas we find bursting in the Bursting Pulsar shuts off *below* a 2–16 keV flux of Eddington fraction of $\sim$0.1 Crab: assuming that the peak persistent luminosity of the Bursting Pulsar was approximately Eddington Limited (e.g. Sazonov et al. 1997), this value corresponds to an Eddington fraction of the order of $\sim$0.1. This suggests that type II bursting in these two objects happens in very different accretion regimes.

Bagnoli et al. (2015) showed that bursting behaviour in the Rapid Burster falls into a number of 'bursting modes', defined by the morphology of individual type II bursts. In particular, they find that type II bursts in the Rapid Burster fall into two classes (see also Marshall, Grindlay & Weisskopf 1979), light curves of which we reproduce in Fig. 21:

(i) Short near-symmetric Bursts with time-scales of tens of seconds and peak rates near the Eddington limit.

(ii) Long bursts with a fast rise, a long $\sim$100 s plateau at peak rate followed by a fast decay. The level of the plateau is generally at or near the Eddington Limit.

Short bursts are very similar in shape to Normal Bursts in the Bursting Pulsar, but we find no analogue of long bursts in our study. Bagnoli et al. (2015) suggest that the 'flat-top' profile of long bursts could be due to the effects of near-Eddington accretion, and they show that the intensity at the 'flat top' of these bursts is close to Eddington limit. Previous works have shown that the persistent emission of the Bursting Pulsar is Eddington-limited at peak, and therefore bursts from the Bursting Pulsar are significantly super-Eddington (Sazonov et al. 1997). We suggest therefore that Long Bursts cannot occur in systems with a persistent rate approaching the Eddington limit. This could explain why Long Bursts are not seen during periods of Normal Bursting in the Bursting Pulsar (during which the persistent emission is $\gtrsim$20 per cent of Eddington), but it remains unclear why these features are not seen later in each outburst when the Bursting Pulsar is fainter. Alternatively, all the differences we see between bursts produced by the Rapid Burster and the Bursting Pulsar could be explained if the physical mechanisms behind these bursts are indeed different between the objects.

Bagnoli et al. (2015) also find a number of correlations between burst parameters in the Rapid Burster, which we can compare with our results for the Bursting Pulsar. We find a number of similarities between the two objects:

(i) The fluence of a burst correlates with its amplitude.

(ii) The duration of a burst does not correlate[12] with the persistent emission.

(iii) The recurrence time between consecutive bursts does not depend on the persistent emission.

There are also a number of differences between the set of correlations between burst parameters in these two systems:

(i) Burst duration is correlated with burst fluence in the Rapid Burster, but these have not been seen to correlate in the Bursting Pulsar.

(ii) Burst duration, peak rate, and burst fluence are all correlated with burst recurrence time in the Rapid Burster. We have not found any of these parameters to correlate with burst recurrence time in the Bursting Pulsar.

(iii) Peak rate and burst fluence correlate with persistent emission in the Bursting Pulsar, but this is not true for bursts of a given type in the Rapid Burster.

As neither the fluence nor the class of a burst in the Rapid Burster depend strongly on persistent emission, which can be used as a proxy for $\dot{M}$, this suggests that the process that triggers type-II bursts in this source is not strongly dependent on the global accretion rate. However, the strong correlations between persistent emission and burst peak and fluence we find in the Bursting Pulsar show that the energetics of individual bursts strongly depend global accretion rate at that time.

It has previously been noted that consecutive Normal Bursts in the Bursting pulsar do not show a strong correlation between recurrence time and fluence (Taam & Lin 1984; Lewin et al. 1996, however see Aptekar et al. 1997). This correlation would be expected if the instability took the form of a relaxation oscillator, as it does in the Rapid Burster (Lewin et al. 1976a). However, we also find that the arrival times of Normal Bursts from the Bursting Pulsar are not consistent with a Poisson distribution with constant mean. This implies either that bursts are also not independent events in the Bursting Pulsar, or that the frequency of these bursts is not constant throughout an outburst as reported by Aptekar et al. (1998).

[12]We state two parameters do not correlate if their Spearman Rank score corresponds to a significance $<3\sigma$.

Downloaded from https://academic.oup.com/mnras/article-abstract/481/2/2273/5086081 by INAF Brera Milano (Osservatorio Astronomico di Brera) user on 20 February 2019

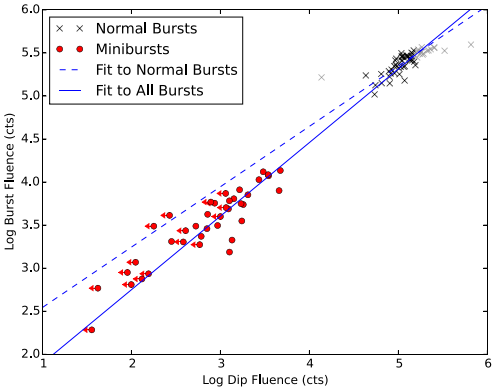

Figure 22. A scatter plot showing the relationship between burst fluence and 'missing' dip fluence for Normal Bursts (black) and Minibursts (Red), with the best-fitting power law plotted in solid blue. A power-law fit to just the Normal Bursts (blue dashed line) also approaches the Minibursts. Note that the Normal Bursts plotted in grey were not used to calculate this latter fit, as the effects of instrumental dead time cause high burst fluences to be underreported. Upper limits on Miniburst dip fluences are shown with arrows.

4.5 Comparison with models of type II bursts

To our knowledge, no models have been proposed which can fully explain type II bursting behaviour, but several models have been proposed in the context of type II bursting from the Rapid Burster MXB 1730-33. A number of models invoke viscous instabilities in the inner disc as the source of cyclical bursting (e.g. Taam & Lin 1984; Hayakawa 1985), but these fail to explain why the majority of Neutron Star LMXBs do not show this behaviour.

Spruit & Taam (1993) use a different approach. They show that, in some circumstances, the interaction between an accretion disc and a rapidly rotating magnetospheric boundary can naturally set up a cycle of discrete accretion events rather than a continuous flow (see also D'Angelo & Spruit 2010, 2012; Scaringi et al. 2017; van den Eijnden et al. 2017). Walker (1992) suggests that, for a neutron star with a radius less than its ISCO, a similar cycle of accretion can be set up when considering the effects of a high radiative torque. All of these models suggest that type II bursts are caused by sporadic accretion events onto the neutron star, which in turn are caused by instabilities that originate in the inner part of the accretion disc. For a more detailed review of these models, see Lewin et al. (1993).

All of the models discussed above are able to reproduce some of the features we see from bursts in the Bursting Pulsar. In particular, the 'dip' we see after Normal Bursts has previously been interpreted as being caused by the inner disc refilling after a sudden accretion event (e.g. Younes et al. 2015). As these dips are also seen after some Minibursts, we could also interpret Minibursts as being caused by a similar cycle. To test this idea, in Fig. 22 we present a scatter plot of the burst and dip fluences for all Normal Bursts and Minibursts. In both classes of burst, there is a strong correlation between these two parameters. We find that a power-law fit to the Normal Bursts in this parameter space also describes the Minibursts. This suggests that the same relationship between burst fluence and missing dip fluence holds for both types of burst, although the two populations are not continuous. This suggests that Minibursts are energetically consistent with being significantly fainter versions of Normal Bursts.

The models of Spruit & Taam (1993) and Walker (1992) also have shortcomings when used to describe the Bursting Pulsar. Walker (1992) states that their model only produces type II bursts for a very specific set of criteria on the system parameters. One of these criteria is an essentially non-magnetic ($B = 0$) neutron star. This is inconsistent with observations of cyclotron lines from the Bursting Pulsar and the presence of a persistent pulsar, which suggest a surface field strength of order 10^{11} G (Doroshenko et al. 2015).

Unlike models based on viscous instability, the model of Spruit & Taam (1993) does not impose a correlation between burst fluence and burst recurrence time (see e.g. the evaluation of this model in the context of the Rapid Burster performed by Bagnoli et al. 2015). However, it does predict a strong correlation between burst recurrence time and mean accretion rate, which is not consistent with our results for the Bursting Pulsar.

In general, we find that models established to explain bursting in the Rapid Burster are poor at explaining bursting in the Bursting Pulsar. Any model which can produce type II bursting in both systems fails to explain why other systems do not also show this behaviour. Our results suggest that type II bursts in the Rapid Burster and the Bursting Pulsar may require two separate models to be explained.

4.5.1 *Evidence of thermonuclear burning*

We also consider the possibility that some of our observations could be explained by thermonuclear burning in the Bursting Pulsar. A thermonuclear origin for the main part of Normal type II X-ray bursts has been ruled out by previous authors (e.g. Lewin et al. 1996), but it is less clear that associated features could not be explained by this process.

It has been shown that, above a certain accretion rate, thermonuclear burning on the surface of a neutron star should be stable; below this rate, thermonuclear burning takes place in the form of type I bursts (e.g. Fujimoto, Hanawa & Miyaji 1981; Bildsten 1995). Bildsten & Brown (1997) have previously studied which form thermonuclear burning on the Bursting Pulsar would take. They find that the presence and profile of a thermonuclear burning event on the Bursting Pulsar would be strongly dependent on both the accretion rate $\dot{M}$ and the magnetic field strength B. They predict that, for $B \gtrsim 3 \times 10^{10}$ G, burning events would take the form of a slowly propagating burning front which would result in a low-amplitude X-ray burst with a time-scale of several minutes. Measurements of the Bursting Pulsar taken during Outburst 3 suggest a surface field strength of $>10^{11}$ G, in turn suggesting that the Bursting Pulsar exists in the regime in which this burning behaviour is possible.

The 'plateau' events after Normal Bursts are consistent with the slow burning predicted by Bildsten & Brown (1997). This picture is consistent with models for type II X-ray bursts involving spasmodic accretion events (e.g. Walker 1992; Spruit & Taam 1993), as plateaus always occur after a type II burst has deposited a large amount of ignitable material onto the neutron star surface. However, in this picture it would be unclear why many Normal Bursts do not show this plateau feature. Mesobursts can also exhibit plateaus, and are therefore may also be products of spasmodic accretion onto the neutron star.

However, the interpretation of Mesobursts as being caused by discrete accretion events is difficult to reconcile with the fact that these features never show dips. Bildsten & Brown (1997) show that, at smaller values of $\dot{M}$, nuclear burning on the Bursting Pulsar could become unstable. Mesobursts are only seen during the latter stages of Outbursts 1 and 2, when the accretion rate is well below 0.1 Eddington. An interesting alternative possibility is that Mesobursts are a hybrid event, consisting of a flash of unstable thermonuclear X-ray burning followed by a slower quasi-stable burning of residual material in the form of a propagating burning front.

Downloaded from https://academic.oup.com/mnras/article-abstract/481/2/2273/5086081 by INAF Brera Milano (Osservatorio Astronomico di Brera) user on 20 February 2019

This picture would also be able to explain why Mesobursts are only seen during the latter parts of each outburst. As the accretion rate onto the Bursting Pulsar approaches Eddington during the peak of its outbursts, it is likely that the accretion rate is high enough that only stable burning is permitted. During the smaller rebrightening events after the main part of each outburst, the accretion rate is ∼1–2 orders of magnitude lower, and hence the system may then be back in the regime in which type I burning is possible. Additional studies of the spectral evolution of Mesobursts will be required to further explore this possibility.

Previous authors have discussed the possibility of a marginally stable burning regime on the surface of neutron stars (not to be confused with the previously mentioned quasi-stable burning). In this regime, which occurs close to the boundary between stable and unstable burning, Heger, Cumming & Woosley (2007) showed that an oscillatory mode of burning may occur. They associated this mode of burning with the mHz QPOs which have been observed in a number of neutron star LMXBs (e.g. Revnivtsev et al. 2001; Altamirano et al. 2008a). These QPOs only occur over a narrow range of source luminosities, show a strong decrease in amplitude at higher energies, and they disappear after a type I burst (e.g. Altamirano et al. 2008a).

Light curves of objects undergoing marginally stable burning qualitatively resemble those of Structured Bursting in the Bursting Pulsar, raising the possibility of a thermonuclear explanation for Structured Bursting. However, as we show in Fig. 4, Structured Bursting during Outburst 1 occurred during a period of time in which the Bursting Pulsar's luminosity changed by ∼1 order of magnitude. In addition to this, in Fig. 17 we show an example of a Mesoburst during a period of Structured Bursting. If Mesobursts can be associated with type I bursts, any marginally stable burning on the surface of the Bursting Pulsar should have stopped after this event. Due to these inconsistencies with observations of marginally stable burning on other sources, it is unlikely that Structured Bursting is a manifestation of marginally stable burning on the Bursting Pulsar.

Linares et al. (2012) observed yet another mode of thermonuclear burning during the 2010 outburst of the LMXB Terzan 5 X-2. They observed a smooth evolution from discrete type I bursts into a period of quasi-periodic oscillations resembling Structured Bursting. This behaviour resembles the evolution we observe between Mesobursts and Structured Bursting in Outbursts 1 and 2 of the Bursting Pulsar (as shown in Fig. 20; compare with fig. 1 in Linares et al. 2012). However, there are a number of differences between the evolutions seen in both objects. In Terzan 5 X-2 the recurrence time-scale of type I bursts during the evolution is strongly related to the accretion rate of the source at the time, whereas there is no such strong relation between the two in Mesobursts from the Bursting Pulsar. Additionally, the quasi-periodic oscillations in Terzan X-2 evolved smoothly back into type I bursts later in the outburst, whereas Structured Bursting does not evolve back into Mesobursts in the Bursting Pulsar. As such, it is unclear that Mesobursts and Structured Bursting can be associated with the unusual burning mode seen on Terzan 5 X-2.

5 CONCLUSIONS

We analyse all X-ray bursts from the Rapid Burster seen by *RXTE*/PCA during its first and second outbursts, as well as bursts seen by other missions during the third outburst of the source. We conclude that these bursts are best described as belonging to four separate classes of burst: Normal Bursts, Mesobursts, Minibursts, and Structured Bursts. We find that the bursting behaviour in these four classes evolves in a similar way throughout the first two outbursts of the Bursting Pulsar. We present a new semimathematical model to fit to the Normal Bursts in this object. Using this new framework, we will be able to better quantify Bursting-Pulsar-like X-ray bursts when they are observed in other objects in the future.

We find the bursts in the Rapid Burster and the Bursting Pulsar to be different in burst profile, peak Eddington ratio, and durations. While the fluence of type II bursts in the Bursting Pulsar depends strongly on the persistent emission at the time, this is not the case in the Rapid Burster. Additionally, the waiting time between bursts in the Rapid Burster depends heavily on the fluence of the preceding burst, but we do not find this in the Bursting Pulsar. Therefore, it would be reasonable to conclude that the bursting in these two objects is generated by two different mechanisms.

However, it is also important to note a number of similarities between the Bursting Pulsar and the Rapid Burster. Bursting behaviour in both objects depends on the global accretion rate of the system and the evolution of its outbursts. For example, the recurrence time of bursts does not depend on persistent emission in either object, and nor does the duration of an individual burst. Notably while type II bursts in the Rapid Burster only occur at luminosities $L \lesssim 0.05 L_{\rm Edd}$, we find that Normal bursts in the Bursting Pulsar only occur at $L \gtrsim 0.1 L_{\rm Edd}$. There is no overlap between the luminosity regimes, in terms of the Eddington Luminosity, at which bursting is observed in the two objects. This leads to the alternative hypothesis that bursts in the two systems may be caused by similar processes, but that these processes take place in very different physical regimes.

ACKNOWLEDGEMENTS

JC thanks the Science and Technology Facilities Council and the Royal Astronomical Society for their financial support. DA thanks the Royal Society, and the International Space Science Institute (*ISSI*) for its support. ND is supported by a Vidi grant from the Dutch Organisation for Scientific Research (NWO). TB acknowledges financial contribution from the agreement ASI-INAF n.2017-14-H.0 between Istituto Nazionale di Astrofisica (INAF) and the Agenzia Spaziale Italiana (ASI).

The authors acknowledge the use of ASTROPY (Astropy Collaboration et al. 2013), NUMPY (Jones et al. 2001), and MATPLOTLIB (Hunter 2007) libraries for PYTHON. We also acknowledge the use of public data from the *RXTE* (Bradt et al. 1993) archive, as well as FTOOLS (Blackburn 1995) for data manipulation. Results provided by the ASM/*RXTE* teams at MIT and at the RXTE Science Operations Facility and Guest Observer Facility at NASA's Goddard Space Flight Centre.

REFERENCES

Altamirano D., van der Klis M., Wijnands R., Cumming A., 2008a, ApJ, 673, L35
Altamirano D., van der Klis M., Méndez M., Jonker P. G., Klein-Wolt M., Lewin W. H. G., 2008b, ApJ, 685, 436
Angelini L., White N. E., Stella L., 1991, ApJ, 371, 332
Aptekar R. L. et al., 1997, Astron. Lett., 23, 147
Aptekar R. L. et al., 1998, ApJ, 493, 404
Archibald A. M. et al., 2009, Science, 324, 1411
Astropy Collaboration, 2013, A&A, 558, A33
Azzalini A., 1985, Scand. J. Stat., 12, 171
Bagnoli T., in't Zand J. J. M., D'Angelo C. R., Galloway D. K., 2015, MNRAS, 449, 268
Bildsten L., 1995, ApJ, 438, 852
Bildsten L., Brown E. F., 1997, ApJ, 477, 897

Downloaded from https://academic.oup.com/mnras/article-abstract/481/2/2273/5086081 by INAF Brera Milano (Osservatorio Astronomico di Brera) user on 20 February 2019

Bildsten L. et al., 1997, ApJS, 113, 367
Blackburn J. K., 1995, in Shaw R. A., Payne H. E., Hayes J. J. E., eds, ASP Conf. Ser. Vol. 77, Astronomical Data Analysis Software and Systems IV. Astron. Soc. Pac., San Francisco, p. 367
Bogdanov S. et al., 2015, ApJ, 806, 148
Bradt H. V., Rothschild R. E., Swank J. H., 1993, A&AS, 97, 355
Burrows D. N. et al., 2003, in Truemper J. E., Tananbaum H. D., eds, Proc. SPIE Conf. Ser. Vol. 4851, X-Ray and Gamma-Ray Telescopes and Instruments for Astronomy. SPIE, Bellingham, p. 1320
Court J., 2017, jmcourt/PANTHEON: Zenodo Release. Available at: https://doi.org/10.5281/zenodo.1040704
Court J. M. C., Altamirano D., Pereyra M., Boon C. M., Yamaoka K., Belloni T., Wijnands R., Pahari M., 2017, MNRAS, 468, 4748
Court J. M. C., Altamirano D., Sanna A., 2018, MNRAS, 477, L106
D'Aì A. et al., 2015, MNRAS, 449, 4288
D'Aì A., Burderi L., Di Salvo T., Iaria R., Pintore F., Riggio A., Sanna A., 2016, MNRAS, 463, L84
D'Angelo C. R., Spruit H. C., 2010, MNRAS, 406, 1208
D'Angelo C. R., Spruit H. C., 2012, MNRAS, 420, 416
Daigne F., Goldoni P., Ferrando P., Goldwurm A., Decourchelle A., Warwick R. S., 2002, A&A, 386, 531
Degenaar N., Wijnands R., Cackett E. M., Homan J., in't Zand J. J. M., Kuulkers E., Maccarone T. J., van der Klis M., 2012, A&A, 545, A49
Degenaar N., Miller J. M., Harrison F. A., Kennea J. A., Kouveliotou C., Younes G., 2014, ApJ, 796, L9
Doroshenko R., Santangelo A., Doroshenko V., Suleimanov V., Piraino S., 2015, MNRAS, 452, 2490
Evans P. A. et al., 2007, A&A, 469, 379
Ferrigno C. et al., 2014, A&A, 567, A77
Finger M. H., Koh D. T., Nelson R. W., Prince T. A., Vaughan B. A., Wilson R. B., 1996, Nature, 381, 291
Fishman G. J., Kouveliotou C., van Paradijs J., Harmon B. A., Paciesas W. S., Briggs M. S., Kommers J., Lewin W. H. G., 1995, IAU Circ., 6272
Fruscione A. et al., 2006, in Proc. SPIE Conf. Ser. Vol. 6270, Observatory Operations: Strategies, Processes, and Systems. SPIE, p. 62701V
Fujimoto M. Y., Hanawa T., Miyaji S., 1981, ApJ, 247, 267
Galloway D. K., Muno M. P., Hartman J. M., Psaltis D., Chakrabarty D., 2008, ApJS, 179, 360
Garmire G. P., Bautz M. W., Ford P. G., Nousek J. A., Ricker G. R., Jr, 2003, in Truemper J. E., Tananbaum H. D., eds, Proc. SPIE Conf. Ser. Vol. 4851, X-Ray and Gamma-Ray Telescopes and Instruments for Astronomy. SPIE, Bellingham, p. 28
Gehrels N., 2004, in Schoenfelder V., Lichti G., Winkler C., eds, ESA SP-552: 5th INTEGRAL Workshop on the INTEGRAL Universe. ESA, Noordwijk, p. 777
Gehrels N., Chipman E., Kniffen D., 1994, ApJS, 92, 351
Giles A. B., Swank J. H., Jahoda K., Zhang W., Strohmayer T., Stark M. J., Morgan E. H., 1996, ApJ, 469, L25
Gosling A. J., Bandyopadhyay R. M., Miller-Jones J. C. A., Farrell S. A., 2007, MNRAS, 380, 1511
Harrison F. A. et al., 2013, ApJ, 770, 103
Hayakawa S., 1985, Phys. Rep., 121, 317
Heger A., Cumming A., Woosley S. E., 2007, ApJ, 665, 1311
Hoffman J. A., Marshall H. L., Lewin W. H. G., 1978, Nature, 271, 630
Hunter J. D., 2007, Comput. Sci. Eng., 9, 90
in't Zand J. J. M., Cumming A., Triemstra T. L., Mateijsen R. A. D. A., Bagnoli T., 2014, A&A, 562, A16
Jahoda K., Swank J. H., Giles A. B., Stark M. J., Strohmayer T., Zhang W., Morgan E. H., 1996, in Siegmund O. H., Gummin M. A., eds, Proc. SPIE Conf. Ser. Vol. 2808, EUV, X-Ray, and Gamma-Ray Instrumentation for Astronomy VII. SPIE, Bellingham, p. 59
Jahoda K., Markwardt C. B., Radeva Y., Rots A. H., Stark M. J., Swank J. H., Strohmayer T. E., Zhang W., 2006, ApJS, 163, 401
Jones E. et al., 2001, SciPy: Open source scientific tools for Python. Available at: http://www.scipy.org/
Kennea J. A., Kouveliotou C., Younes G., 2014, Astron. Telegram, 5845
Kouveliotou C., van Paradijs J., Fishman G. J., Briggs M. S., Kommers J., Harmon B. A., Meegan C. A., Lewin W. H. G., 1996, Nature, 379, 799
Koyama K. et al., 2007, PASJ, 59, 23
Krimm H. A. et al., 2013, ApJS, 209, 14
Lamb D. Q., Miller M. C., Taam R. E., 1996, AAS, 28, 960
Levine A. M., Bradt H., Cui W., Jernigan J. G., Morgan E. H., Remillard R., Shirey R. E., Smith D. A., 1996, ApJ, 469, L33
Lewin W. H. G. et al., 1976a, ApJ, 207, L95
Lewin W. H. G., Clark G., Doty J., 1976b, IAU Circ., 2922
Lewin W. H. G., van Paradijs J., Taam R. E., 1993, Space Sci. Rev., 62, 223
Lewin W. H. G., Rutledge R. E., Kommers J. M., van Paradijs J., Kouveliotou C., 1996, ApJ, 462, L39
Linares M., Altamirano D., Chakrabarty D., Cumming A., Keek L., 2012, ApJ, 748, 82
Linares M., Kennea J., Krimm H., Kouveliotou C., 2014, Astron. Telegram, 5883
Lubiński P., 2009, A&A, 496, 557
Marshall H., Grindlay J., Weisskopf M., 1979, in Bulletin of the American Astronomical Society. p. 788
Masetti N., D'Avanzo P., Blagorodnova N., Palazzi E., 2014, Astron. Telegram, 5999
Mitsuda K. et al., 2007, PASJ, 59, 1
Negoro H. et al., 2014, Astron. Telegram, 5790
Paciesas W. S., Harmon B. A., Fishman G. J., Zhang S. N., Robinson C. R., 1996, IAU Circ., 6284
Papitto A. et al., 2013, Nature, 501, 517
Patruno A., Maitra D., Curran P. A., D'Angelo C., Fridriksson J. K., Russell D. M., Middleton M., Wijnands R., 2016, ApJ, 817, 100
Poisson S., 1837, Mathematics of Statistics, Bachelier. Available at: https://books.google.co.uk/books?id=uB8OAAAAQAAJ
Rappaport S., Joss P. C., 1997, ApJ, 486, 435
Revnivtsev M., Churazov E., Gilfanov M., Sunyaev R., 2001, A&A, 372, 138
Sanna A. et al., 2017a, MNRAS, 469, 2
Sanna A., D'Ai A., Bozzo E., Riggio A., Pintore F., Burderi L., Di Salvo T., Iaria R., 2017b, Astron. Telegram, 10079
Sazonov S. Y., Sunyaev R. A., Lund N., 1997, Astron. Lett., 23, 286
Scaringi S., Maccarone T. J., D'Angelo C., Knigge C., Groot P. J., 2017, Nature, 552, 210
Spruit H. C., Taam R. E., 1993, ApJ, 402, 593
Strohmayer T., Bildsten L., 2006, in Lewin W., van der Klis M., eds, Compact stellar X-ray sources. Cambridge Univ. Press, Cambridge, p. 113
Strohmayer T. E., Jahoda K., Giles A. B., Lee U., 1997, ApJ, 486, 355
Sturner S. J., Dermer C. D., 1996, ApJ, 465, L31
Sturner S. J., Shrader C. R., 2005, ApJ, 625, 923
Taam R. E., Lin D. N. C., 1984, ApJ, 287, 761
Tan J., Lewin W. H. G., Lubin L. M., van Paradijs J., Penninx W., van der Klis M., Damen E., Stella L., 1991, MNRAS, 251, 1
Tomsick J. A., Kalemci E., Corbel S., Kaaret P., 2003, ApJ, 592, 1100
Uchiyama Y. et al., 2008, PASJ, 60, S35
van den Eijnden J., Bagnoli T., Degenaar N., Lohfink A. M., Parker M. L., in't Zand J. J. M., Fabian A. C., 2017, MNRAS, 466, L98
Walker M. A., 1992, ApJ, 385, 651
Weisskopf M. C., 1999, AAS, 31, 1514
Wijnands R., Wang Q. D., 2002, ApJ, 568, L93
Wijnands R., Méndez M., Markwardt C., van der Klis M., Chakrabarty D., Morgan E., 2001, ApJ, 560, 892
Winkler C. et al., 2003, A&A, 411, L1
Woods P. M. et al., 1999, ApJ, 517, 431
Woods P. M., Kouveliotou C., van Paradijs J., Koshut T. M., Finger M. H., Briggs M. S., Fishman G. J., Lewin W. H. G., 2000, ApJ, 540, 1062
Younes G. et al., 2015, ApJ, 804, 43

APPENDIX A: LIST OF *RXTE* OBSERVATIONS

In Table A1, we present a table of all *RXTE* observations used in this study. The prefixes **A**, **B**, **C**, **D**, and **E** correspond to OBSIDs beginning with 10401-01, 20077-01, 20078-01, 20401-01, and 30075-01, respectively.

Downloaded from https://academic.oup.com/mnras/article-abstract/481/2/2273/5086081 by INAF Brera Milano (Osservatorio Astronomico di Brera) user on 20 February 2019

Table A1. A list of all *RXTE* observations of the Bursting Pulsar used in this study. Exposure is given in seconds, and date is given in days from MJD 50000. The prefixes **A**, **B**, **C**, **D**, and **E** correspond to OBSIDs beginning with 10401-01, 20077-01, 20078-01, 20401-01, and 30075-01, respectively.

Obsid	Exp.	Date	Obsid	Exp.	Date	Obsid	Exp.	Date	Obsid	Exp.	Date	Obsid	Exp.	Date
A-01-00	3105	119	**A**-57-00	2432	250	**A**-94-00	3216	332	**C**-16-00	4941	562	**C**-40-01	3419	730
A-02-00	1655	117	**A**-57-01	894	253	**A**-95-00	9487	333	**C**-16-01	671	561	**C**-40-02	896	764
A-03-00	6724	122	**A**-57-02	1408	253	**A**-96-00	2627	337	**C**-16-02	1159	562	**C**-41-00	5255	735
A-03-000	2372	122	**A**-57-03	1792	253	**A**-97-00	3341	340	**C**-17-00	3537	568	**C**-41-01	2387	735
A-03-01	768	122	**A**-58-00	1024	255	**A**-98-00	99	343	**C**-18-00	2981	576	**C**-41-02	1141	744
A-04-00	639	128	**A**-58-01	1401	255	**A**-99-00	2783	345	**C**-18-01	3103	576	**C**-42-00	1476	744
A-05-00	1990	129	**A**-58-02	1679	255	**A**-99-01	1001	344	**C**-19-00	3286	582	**C**-43-00	5277	764
A-06-00	1280	134	**A**-58-03	1683	255	**B**-01-00	1664	467	**C**-19-01	2893	582	**C**-44-00	6712	769
A-08-00	2431	142	**A**-59-00	1152	257	**B**-02-00	1920	468	**C**-19-02	470	582	**D**-01-00	2688	523
A-09-00	640	138	**A**-59-01	2203	257	**B**-03-00	2982	469	**C**-20-00	3460	589	**D**-02-00	3469	525
A-10-00	2470	143	**A**-59-02	768	257	**B**-04-00	3530	470	**C**-20-01	1126	589	**D**-03-00	3026	528
A-11-00	2381	148	**A**-60-00	1907	260	**B**-05-00	2025	472	**C**-21-00	3659	596	**D**-04-00	3050	531
A-12-00	3352	151	**A**-60-01	3376	260	**B**-06-00	2677	473	**C**-21-01	2907	596	**D**-05-00	3485	536
A-13-00	3480	155	**A**-60-02	1783	260	**B**-07-00	3365	473	**C**-21-02	1086	596	**D**-06-00	1367	538
A-14-00	1839	158	**A**-60-03	1559	260	**B**-08-00	3113	475	**C**-22-00	1967	602	**D**-07-00	3196	543
A-15-00	1595	161	**A**-61-00	3292	262	**B**-09-00	2868	480	**C**-22-01	3086	602	**D**-08-00	2617	548
A-16-00	3470	156	**A**-61-01	3035	262	**B**-10-00	1009	482	**C**-22-02	1024	602	**D**-09-00	2598	553
A-17-00	4481	164	**A**-61-02	2013	262	**B**-11-00	2864	487	**C**-23-00	3697	607	**D**-10-00	4069	560
A-18-00	384	171	**A**-62-00	2390	264	**B**-12-00	1847	489	**C**-23-01	3091	607	**D**-11-00	2686	572
A-19-00	128	172	**A**-62-01	1703	264	**B**-13-00	2805	497	**C**-24-00	1152	618	**D**-12-00	2867	565
A-20-00	2087	178	**A**-62-02	2719	264	**B**-14-00	3741	499	**C**-24-01	2300	618	**D**-13-00	2021	585
A-21-00	2711	181	**A**-63-00	517	266	**B**-15-00	384	501	**C**-24-02	1386	618	**D**-13-01	765	585
A-22-00	2816	183	**A**-63-01	3077	266	**B**-16-00	768	503	**C**-25-00	4069	626	**D**-14-00	2640	594
A-22-01	2911	185	**A**-64-00	2381	268	**B**-17-00	2399	509	**C**-25-01	1920	626	**D**-14-01	1719	594
A-23-00	1678	187	**A**-64-01	3110	268	**B**-18-00	2306	511	**C**-25-02	768	626	**D**-15-00	3226	621
A-24-00	2509	189	**A**-65-00	2003	270	**B**-19-00	3477	516	**C**-26-00	2071	633	**D**-15-01	1373	621
A-25-00	2846	192	**A**-65-01	2744	270	**B**-20-00	1922	520	**C**-26-01	4043	633	**D**-16-00	2432	609
A-26-00	768	194	**A**-65-02	4331	270	**C**-01-00	8200	389	**C**-27-00	1792	638	**D**-16-01	1562	609
A-27-00	2923	196	**A**-66-00	2203	272	**C**-02-00	1408	400	**C**-27-01	2495	638	**D**-17-00	1790	628
A-28-00	6839	199	**A**-66-01	1723	272	**C**-02-01	896	401	**C**-27-02	3082	638	**D**-17-01	1291	628
A-29-00	3478	201	**A**-66-02	2533	272	**C**-02-02	512	401	**C**-28-00	3454	644	**D**-18-00	1959	641
A-30-00	5906	203	**A**-67-00	395	274	**C**-03-00	3409	465	**C**-28-01	1359	644	**D**-18-01	2614	641
A-31-00	6170	206	**A**-67-01	3533	274	**C**-03-01	2635	466	**C**-28-02	756	644	**D**-19-00	3158	650
A-32-00	2712	209	**A**-67-02	3466	274	**C**-03-02	2645	466	**C**-29-00	1535	652	**D**-20-00	751	672
A-34-00	1831	213	**A**-68-00	1841	276	**C**-04-00	2620	478	**C**-30-01	3435	658	**E**-01-00	512	831
A-35-00	2563	216	**A**-69-00	3659	278	**C**-04-01	2956	477	**C**-31-00	1920	662	**E**-02-00	1836	845
A-36-00	3683	219	**A**-70-00	2022	280	**C**-04-02	2515	476	**C**-31-01	1152	662	**E**-03-00	1871	859
A-37-00	3446	215	**A**-71-00	3474	283	**C**-05-00	1421	484	**C**-31-02	1012	657	**E**-04-00	1927	873
A-38-00	1536	217	**A**-72-00	5687	285	**C**-05-01	1995	484	**C**-32-00	4646	678	**E**-05-00	2088	889
A-39-00	2317	218	**A**-73-00	3109	287	**C**-05-02	2505	485	**C**-32-01	2803	678	**E**-06-00	2003	901
A-40-00	1239	220	**A**-74-00	1659	289	**C**-06-00	2770	492	**C**-33-00	4334	747	**E**-07-00	1536	914
A-41-00	1363	221	**A**-75-00	1798	291	**C**-06-01	2375	492	**C**-33-01	3534	748	**E**-08-00	967	935
A-42-00	2728	224	**A**-76-00	1558	293	**C**-06-02	2203	492	**C**-33-02	2957	748	**E**-09-00	1598	949
A-43-00	2079	225	**A**-77-00	1738	295	**C**-07-00	1258	494	**C**-34-00	3477	687	**E**-10-00	1835	961
A-44-00	2076	226	**A**-78-00	463	297	**C**-08-00	3305	505	**C**-34-01	1008	687	**E**-11-00	1741	975
A-45-00	2050	228	**A**-79-00	1024	299	**C**-08-01	777	505	**C**-34-02	2831	687	**E**-12-00	1032	991
A-47-00	2687	232	**A**-80-00	5818	301	**C**-09-00	1377	513	**C**-35-00	1497	756	**E**-13-00	1231	1001
A-48-00	2267	234	**A**-81-00	6898	303	**C**-09-01	1536	513	**C**-35-01	1959	755	**E**-14-00	1608	1016
A-49-00	35	236	**A**-82-00	3537	306	**C**-10-00	1664	517	**C**-35-02	2023	755	**E**-15-00	1712	1030
A-50-00	3719	238	**A**-83-00	512	308	**C**-10-01	3796	518	**C**-36-00	2825	702	**E**-16-00	1440	1045
A-51-00	3590	240	**A**-84-00	6361	310	**C**-11-00	2330	527	**C**-36-01	1592	702	**E**-17-00	1888	1057
A-52-00	2518	241	**A**-85-00	10391	312	**C**-11-01	290	527	**C**-37-00	2092	709	**E**-18-00	1847	1071
A-53-00	3063	243	**A**-86-00	9232	314	**C**-11-02	2399	527	**C**-37-01	384	710	**E**-19-00	1792	1086
A-55-00	3328	245	**A**-87-00	3109	316	**C**-12-00	3345	534	**C**-38-00	1752	716	**E**-20-00	1904	1101
A-55-01	3395	245	**A**-88-00	6630	318	**C**-12-01	2048	534	**C**-38-01	1536	716	**E**-21-00	1921	1115
A-55-02	2667	245	**A**-89-00	2569	320	**C**-13-00	1735	541	**C**-38-02	1144	716	**E**-22-00	1769	1129
A-56-00	512	250	**A**-90-00	2209	323	**C**-13-01	1691	541	**C**-38-03	338	717	**E**-23-00	1892	1135
A-56-01	1280	250	**A**-91-00	2317	325	**C**-14-00	3579	549	**C**-39-00	2756	723	**E**-24-00	1943	1197
A-56-02	1664	250	**A**-92-00	2199	327	**C**-14-01	2785	549	**C**-39-01	4690	723	**E**-25-00	2237	1210
A-56-03	1920	250	**A**-93-00	3720	331	**C**-15-00	7494	579	**C**-40-00	3419	730	**E**-26-00	1396	1224

Downloaded from https://academic.oup.com/mnras/article-abstract/481/2/2273/5086081 by INAF Brera Milano (Osservatorio Astronomico di Brera) user on 20 February 2019

APPENDIX B: NORMAL BURST HISTOGRAMS

In Figs B1–B10, we present histograms showing the distributions of ϕ_B, a_B, σ_B, c, ϕ_d, a_d, d, λ, ϕ_p, and a_p we find in our population study. Each of these is a parameter we used to fit the Normal Bursts in our sample: see Section 3.3.2 for a full explanation of these parameters. In Figs B11–B16, we show the distributions of ϕ_B, a_B, ϕ_d, a_d, ϕ_p, and a_p after being normalized by the persistent emission rate k at the time of each burst.

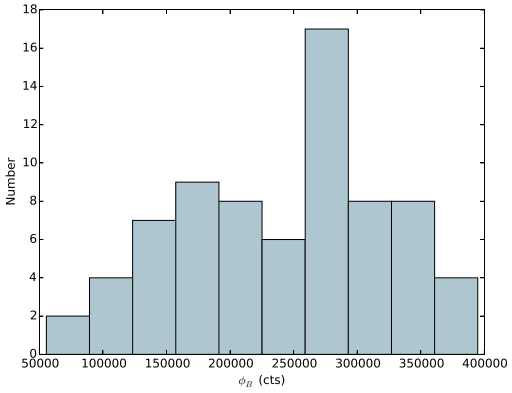

Figure B1. A histogram showing the distribution of burst fluence ϕ_B amongst our sample of Normal Bursts.

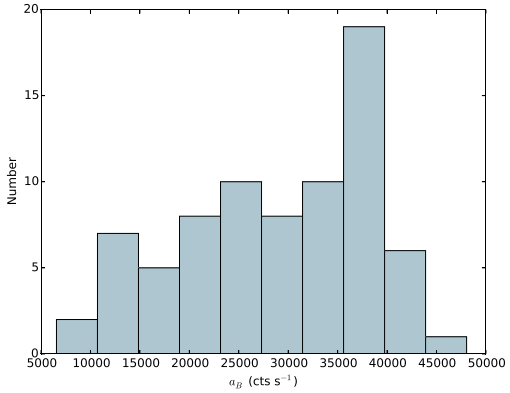

Figure B2. A histogram showing the distribution of burst amplitude a_B amongst our sample of Normal Bursts.

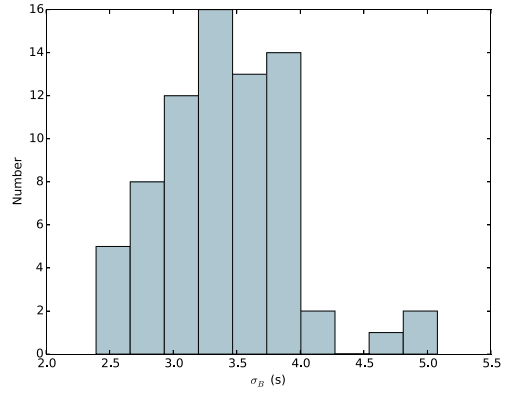

Figure B3. A histogram showing the distribution of burst width σ_B amongst our sample of Normal Bursts.

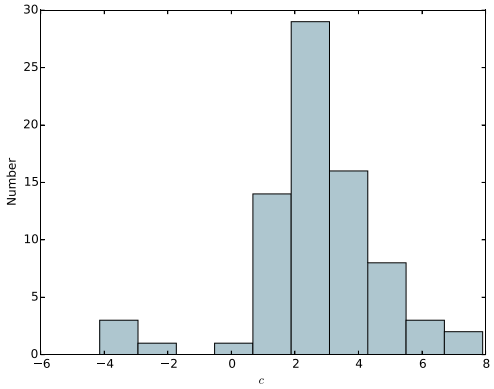

Figure B4. A histogram showing the distribution of burst skewness c amongst our sample of Normal Bursts.

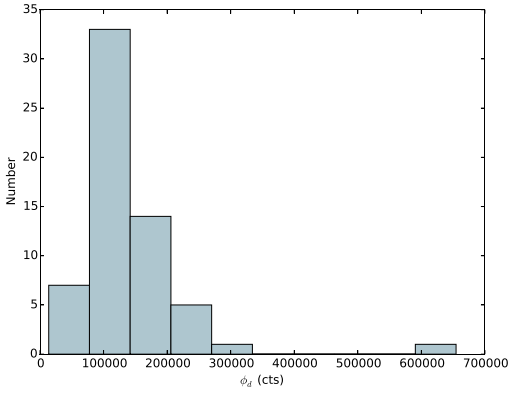

Figure B5. A histogram showing the distribution of dip fluence ϕ_d amongst our sample of Normal Bursts.

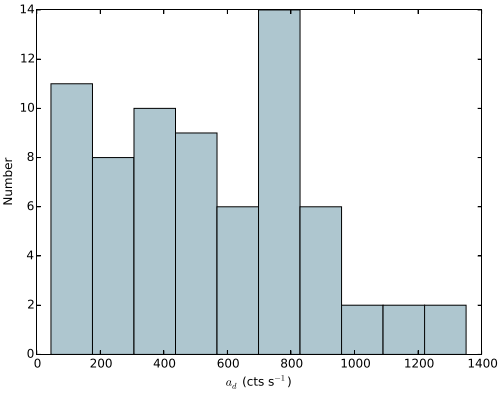

Figure B6. A histogram showing the distribution of dip amplitude a_d amongst our sample of Normal Bursts.

Downloaded from https://academic.oup.com/mnras/article-abstract/481/2/2273/5086081 by INAF Brera Milano (Osservatorio Astronomico di Brera) user on 20 February 2019

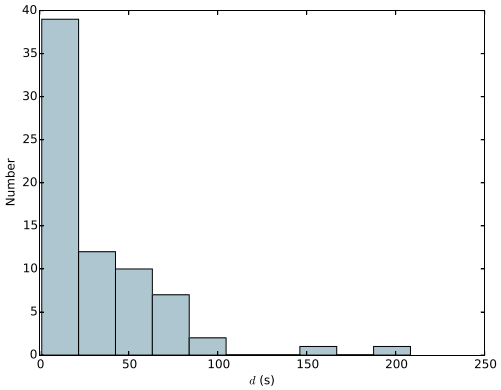

Figure B7. A histogram showing the distribution of dip fall-time d amongst our sample of Normal Bursts.

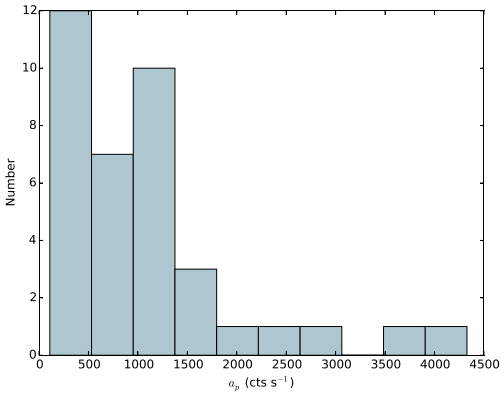

Figure B10. A histogram showing the distribution of plateau amplitude a_p amongst our sample of Normal Bursts.

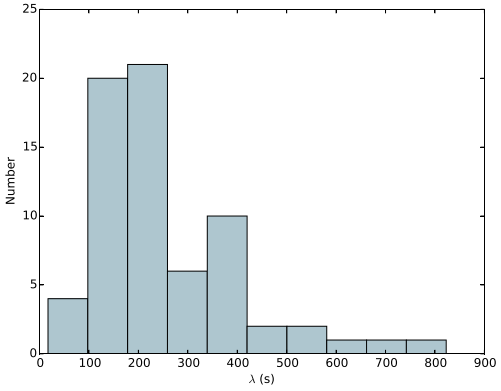

Figure B8. A histogram showing the distribution of dip recovery time-scale λ amongst our sample of Normal Bursts.

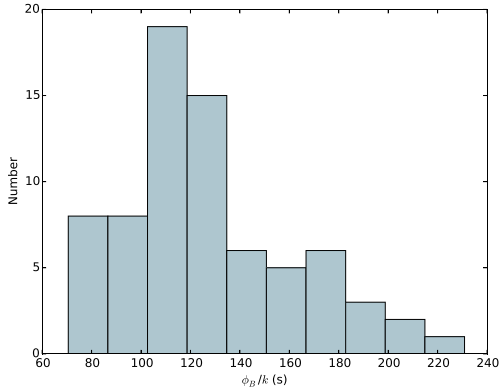

Figure B11. A histogram showing the distribution of persistent-emission-normalized burst fluence ϕ_B/k amongst our sample of Normal Bursts.

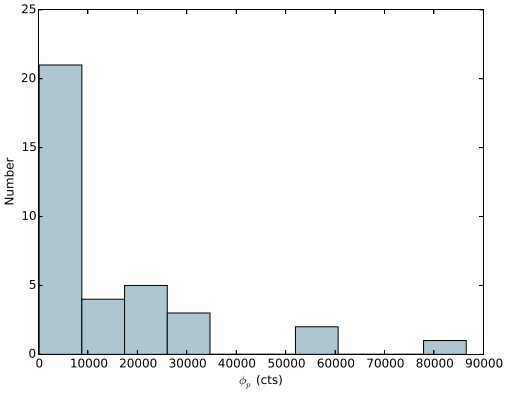

Figure B9. A histogram showing the distribution of plateau fluence ϕ_p amongst our sample of Normal Bursts.

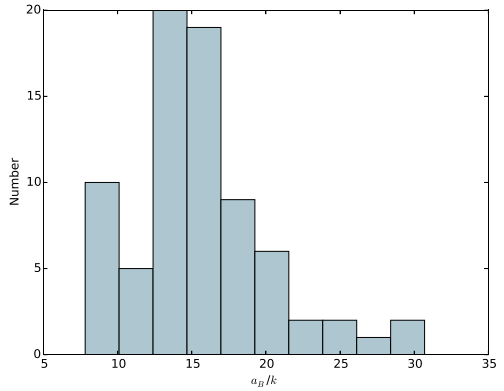

Figure B12. A histogram showing the distribution of persistent-emission-normalized burst amplitude a_B/k amongst our sample of Normal Bursts.

Downloaded from https://academic.oup.com/mnras/article-abstract/481/2/2273/5086081 by INAF Brera Milano (Osservatorio Astronomico di Brera) user on 20 February 2019

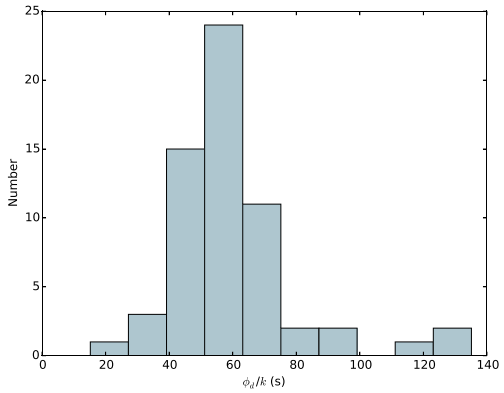

Figure B13. A histogram showing the distribution of persistent-emission-normalized dip fluence ϕ_d/k amongst our sample of Normal Bursts.

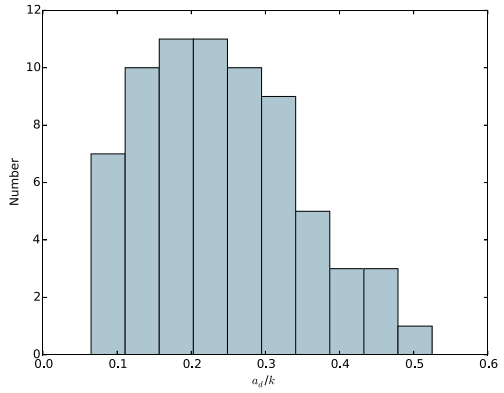

Figure B14. A histogram showing the distribution of persistent-emission-normalized dip amplitude a_d/k amongst our sample of Normal Bursts.

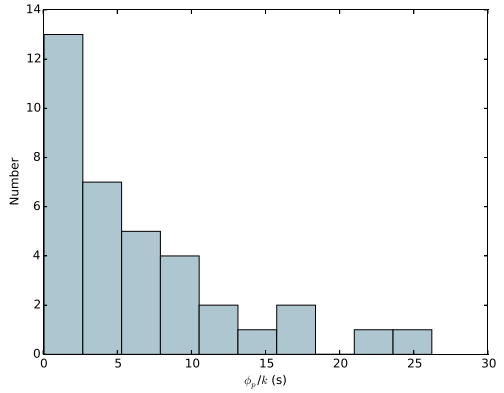

Figure B15. A histogram showing the distribution of persistent-emission-normalized plateau fluence ϕ_p/k amongst our sample of Normal Bursts.

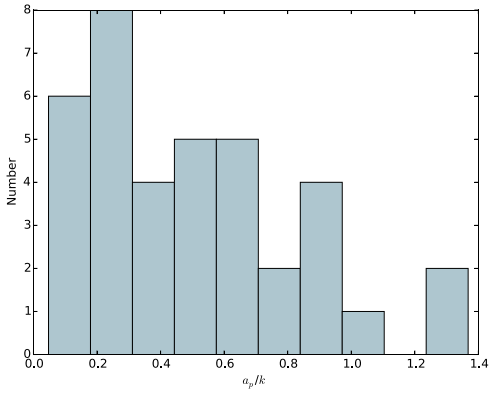

Figure B16. A histogram showing the distribution of persistent-emission-normalized plateau amplitude a_p/k amongst our sample of Normal Bursts.

APPENDIX C: PARAMETER CORRELATIONS IN NORMAL BURSTS

Before normalizing for persistent rate, we find $>5\,\sigma$ correlations between 12 pairs of the parameters we use to describe Normal Bursts:

(i) Persistent emission k correlates with burst fluence ϕ_B ($>10\,\sigma$), burst amplitude a_b ($>10\,\sigma$), dip fluence ϕ_D ($>10\,\sigma$), and dip amplitude a_d ($7.2\,\sigma$).

(ii) Burst fluence ϕ_B also correlates with burst amplitude a_B ($>10\,\sigma$), dip fluence ϕ_D ($>10\,\sigma$), and dip amplitude a_d ($7.1\,\sigma$).

(iii) Burst amplitude ϕ_B also correlates with dip fluence ϕ_D ($6.2\,\sigma$) and dip amplitude a_d ($5.7\,\sigma$).

(iv) Burst width σ_B correlates with burst skewness c ($5.8\,\sigma$).

(v) Dip amplitude a_d anticorrelates with dip recovery time-scale λ ($5.0\,\sigma$).

(vi) Plateau fluence ϕ_p correlates with plateau amplitude a_p ($6.6\,\sigma$).

The full correlation matrix can be found in Fig. C1, in which these pairs with $>5\,\sigma$ correlations are highlighted.

Downloaded from https://academic.oup.com/mnras/article-abstract/481/2/2273/5086081 by INAF Brera Milano (Osservatorio Astronomico di Brera) user on 20 February 2019

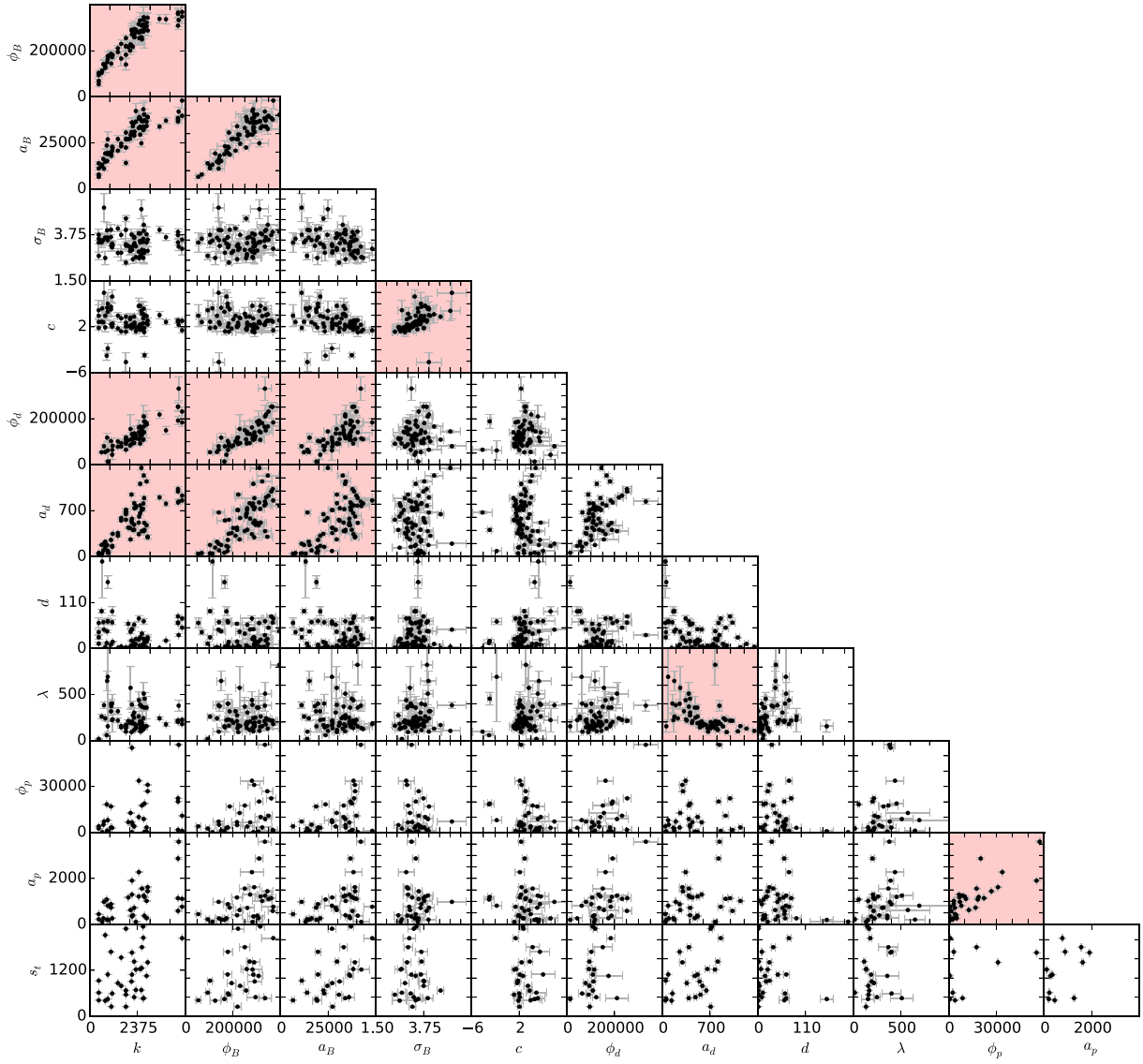

Figure C1. Covariance Matrix with a scatter plot of each of the 66 pairings of the 12 Normal Burst parameters listed in Section 3.3.4. Pairings that show a correlation using the Spearman Rank metric with a significance $\geq 5\,\sigma$ are highlighted in red.

This paper has been typeset from a TEX/LATEX file prepared by the author.

Downloaded from https://academic.oup.com/mnras/article-abstract/481/2/2273/5086081 by INAF Brera Milano (Osservatorio Astronomico di Brera) user on 20 February 2019